












Article

# Validation and Application of the Accu-Waves Operational Platform for Wave Forecasts at Ports

Christos Makris <sup>1,\*</sup> , Andreas Papadimitriou <sup>2,3</sup>, Vasilis Baltikas <sup>1</sup> , Giannis Spiliopoulos <sup>4,5</sup> , Yiannis Kontos <sup>1</sup> , Anastasios Metallinos <sup>2,3</sup>, Yannis Androulidakis <sup>1</sup> , Michalis Chondros <sup>2</sup> , Georgios Klonaris <sup>6</sup> , Dimitra Malliouri <sup>2</sup> , Nikolaos Nagkoulis <sup>1</sup> , Dimitris Zissis <sup>4,5</sup> , Vasiliki Tsoukala <sup>2</sup>, Theophanis Karambas <sup>1</sup>  and Constantine Memos <sup>2</sup>

<sup>1</sup> School of Civil Engineering, Aristotle University of Thessaloniki, 54124 Thessaloniki, Greece; vmpaltik@civil.auth.gr (V.B.); ykontos@civil.auth.gr (Y.K.); iandroul@civil.auth.gr (Y.A.); nikolaosn@civil.auth.gr (N.N.); karambas@civil.auth.gr (T.K.)

<sup>2</sup> School of Civil Engineering, National Technical University of Athens, 15773 Athens, Greece; andrewnt@mail.ntua.gr (A.P.); michondros@gmail.com (M.C.); dimalliouri@gmail.com (D.M.); tsoukala@mail.ntua.gr (V.T.); memos-ports@civil.ntua.gr (C.M.)

<sup>3</sup> Scientia Maris, Chalandri, 15234 Athens, Greece

<sup>4</sup> MarineTraffic, 11525 Athens, Greece; gspiliopoulos@aegean.gr (G.S.); dzissis@aegean.gr (D.Z.)

<sup>5</sup> School of Engineering, University of the Aegean, 84100 Ermoupolis, Greece

<sup>6</sup> Department of Geography, Ghent University, 9000 Ghent, Belgium; georgeklo1@hotmail.com

\* Correspondence: cmakris@civil.auth.gr

**Abstract:** This paper presents a recently developed Operational Forecast Platform (OFP) for prevailing sea conditions at very important ports worldwide (Accu-Waves). The OFP produces reliable high-resolution predictions of wave characteristics in and around ocean ports. Its goal is to support safer navigation, predict possible port downtime, assist vessel approaching, enhance management of towing services, and bolster secure ship maneuvering in busy ports around the globe. Accu-Waves OFP is based on integrated, high-resolution wave modelling over the continental shelf and in coastal areas that incorporates data from global- and regional-scale, open-sea wave and ocean circulation forecasts as boundary conditions. The coupling, nesting, calibration, and implementation of the models are reported and discussed in this paper, concerning 50 selected areas near and inside significant port basins. The detailed setup of the Accu-Waves OFP and its sub-system services is also provided regarding three-day forecasts at three-hourly intervals. The validation of the wave forecast system against in situ observations from wave buoys in coastal areas of the USA, Belgium, and Spain, as well as other model predictions by established OFPs, seems very promising, with performance skill scores ranging from adequate to very good. An exceptional case of stormy seas under severe marine weather conditions with very high wave maxima (>10 m) in the port of Algeciras is further discussed, confirming the good performance of the Accu-Waves OFP.

**Keywords:** wave modelling; operational forecast; ports; TOMAWAC; WAVE-L; downscaling; marine weather prediction; web-GIS; port engineering; navigation safety



**Citation:** Makris, C.; Papadimitriou, A.; Baltikas, V.; Spiliopoulos, G.; Kontos, Y.; Metallinos, A.; Androulidakis, Y.; Chondros, M.; Klonaris, G.; Malliouri, D.; et al. Validation and Application of the Accu-Waves Operational Platform for Wave Forecasts at Ports. *J. Mar. Sci. Eng.* **2024**, *12*, 220. <https://doi.org/10.3390/jmse12020220>

Academic Editors: Pietro Scandura and Christos Stefanakos

Received: 9 December 2023

Revised: 12 January 2024

Accepted: 23 January 2024

Published: 25 January 2024



**Copyright:** © 2024 by the authors. Licensee MDPI, Basel, Switzerland. This article is an open access article distributed under the terms and conditions of the Creative Commons Attribution (CC BY) license (<https://creativecommons.org/licenses/by/4.0/>).

## 1. Introduction

Seaports are identified as the most essential hubs for global economic development that hinges on world trade, according to 'Blue Economy' goals set during the last decade [1]. Harbor and port infrastructures provide access and services to the global maritime industry, i.e., both coastal short-sea shipping and intercontinental cross-ocean shipping, thus feeding and supporting the worldwide supply chains. 40% of the world's population resides in coastal areas, and 80% of the world trade volume is carried by port-to-port marine pathways [2]. They are integral to maritime transport services, as well as the fisheries' industry, the support of offshore energy transit and intercontinental fuel transport, and

many other crucial political and economic activities that take place in the coastal zone (e.g., travel, security, military action, etc.). Seaports also provide vital socioeconomic linkages and are key to regional and inter-island connectivity, serving tourism, journeying, recreation, athletic events, etc. Hence, they are designed to enable the safe, speedy loading and unloading of vessels at the interchange point for sea and land freight. Nevertheless, adverse environmental conditions, such as episodic rising sea levels and extreme storm waves, can severely impact the harbor protection infrastructure and cause port service downtime. This may negatively affect the smooth flow of local, regional, and global marine traffic. Some port authorities, especially in harbors built inside rivers and estuaries or deltas (e.g., London, Hamburg, etc.), have taken precautionary action, such as tidal barriers, movable flood defenses, and expanded or upgraded breakwaters against storm surge and wave attack, respectively, on the entrances of navigational channels and port areas [3,4].

Furthermore, the possible effects of climate change are estimated to cause an increase in Sea Level Rise (SLR) in the 21st century [5], probably also causing the rise of the aforementioned threats in the future. The impact of projected climate change on the ocean shipping industry may not be easy to define regarding induced changes in traffic lanes, nautical routes, coastal waypoints, and navigation pathways in port approaches. However, the impacts on shipping vessels calling at existing harbor facilities are already evident, while the Mean Sea level (MSL) is rising, which can boost the negative effects of high waves and storm tides in port areas [6].

### 1.1. Theme of Research

Seaport resilience and other critical maritime transport infrastructure are crucial to the 2030 Agenda for Sustainable Development (e.g., goals 9, 13, 14, and target 1.5), the Paris Agreement, the New Urban Agenda, and the Sendai Framework for Disaster Risk Reduction (DRR). In this framework, the Early Warning Systems (EWSs) play a very important role in navigation safety [7] by predicting hazards and assisting in the mitigation of their impacts, such as coastal infrastructure damage or destruction, ship accidents (human and property losses), and port downtime or transportation delays (vessel approach stoppage, halt of berth-load-dredge operations, etc.) due to rough sea conditions. PIANC [8] has produced several reports on the climate-related risks of ports and waterways around the world due to the increase in the frequency and intensity of severe weather events, leading to storm track shifts, rising sea levels, and changes in seasonal wind patterns and wave conditions. All these may pose a significant risk to the shipping business, port operations, harbor safety, and coastal infrastructure—and hence to local, national, and global economies. Port and waterway operators, managing waterborne transport in coastal areas, need to strengthen the resilience of harbors and adapt to a four-stage methodological framework [8]:

- (a) Identify assets, operations, and systems affected by severe marine weather supported by reliable local-scale met-ocean weather prediction.
- (b) Urgent setup of local-scale high-resolution wave modelling (and monitoring).
- (c) On-the-fly decision-making is based on forecasted hazards in terms of waterborne transport vulnerability and risk assessment.
- (d) Conceptual design of combating marine weather hazards by screening and evaluating adaptation pathways.

US ports have only recently begun resiliency planning against climate change effects [9,10], yet there is still a general lack of standards and mandates in terms of EWS (a first-level measure of preparedness against more extreme marine weather events and related coastal hazards) for most of them.

The initial inexpensive approach to coastal hazard adaptation and resilience planning for ports is the development of a reliable Operational Forecast Platform (OFP) supporting local-scale EWSs around the world. During the last two decades, the short-term (ranging from several hours to a few days) sea-state forecasts have become more reliable, reaching quite adequate accuracy levels. Recent advances in numerical predictions for met-ocean parameters have enabled the development of operational forecasting systems able to

provide accurate perspectives of near-future marine weather conditions and consequent support of decision-making processes concerning seakeeping in ports and navigation safety (see following Section 1.2 for a non-exhausting list of references). The need for operational sea-state forecast platforms and web applications is demonstrated by the International Maritime Organization's (IMO) strategy under *e*-Navigation [11]. The latter has set the goal of reducing environmental adverse effects and human errors on navigation safety through digital analysis and data dissemination [7]. Therefore, the IMO [12] indicates the need for more accurate, high-resolution meteorological and hydrographic data as one of the main electronic products required in the Strategic Plan 2015–2019 for Local Port Services, including seakeeping information at mooring positions [8].

Hence, we hereby present a recently built OFP that aspires to assist harbor-related stakeholders (port authorities and managers, shipping industry, etc.) to reliably predict and identify in detail any possible impact areas due to storm waves and high seas in order to help decision-making related to the ocean freight industry, port infrastructure, ship trading routes, and navigation pathways at port approaches [13–18]. OFPs for marine conditions in the open sea and coastal areas (the former producing essential information about the boundary conditions of the latter) involve the implementation of wave model predictions with the highest feasible resolution. Validation of the utilized models ensues as a main theme of research [19]. For these OFPs to be reliable, robust, and effective in terms of computational cost, they usually focus on a few or frequently only one pilot study area, referring to a single port and its surrounding natural and built coastal area. This may be insufficient for the needs of the global-perspective shipping industry, as vessel owners, companies, and navigators should refer to many different products and services in a very diverse way to provide all the necessary information, while we hereby propose a unified approach to achieve so in several important ports worldwide.

### 1.2. Literature Review

To this end, Rogers et al. [20] produced validated forecasts and hindcasts for spectral waves with the Simulating WAVes Nearshore (SWAN) model in the Southern California Bight in support of the Nearshore Canyon Experiment (NCEX) field program, discussing discrepancies of bathymetric and topographic resolution in shallow and island areas. Allard et al. [21] presented a Portuguese case study about a real-time nearshore prediction system incorporating input from global meteorological and oceanographic forecasts as boundary and forcing conditions. Dykes et al. [22] evaluated a high-resolution OFP for waves in the Adriatic Sea, incorporating SWAN to model high waves during storms due to Bora and Sirocco winds, with good prediction skills only in offshore areas. Singhal et al. [23] presented a three-way coupled Wave Forecast System (WFS) for the support of marine operations in the USA's Prince William Sound with good model forecast skill for open sea rather than nearshore areas. The large-scale wave forecasts of the European Centre for Medium-Range Weather Forecasts (ECMWF) with WAM (WAVE Modelling) Cycle 4 have been discussed [24], yet again in the open ocean away from coastal and port areas. Chawla et al. [25] set a new paradigm in wave OFPs for the National Centre for Environmental Prediction (NCEP) using the WAVEWATCH-III model in two-way nested mode to achieve adequate grid resolution for multiple areas and forecast products. Rusu and Soares [26–28] attempted to validate a high-resolution SWAN model system for wave forecasting in port approaches of Portuguese coastal areas, including offshore white-capping and data assimilation [29]. Sandhya et al. [30] demonstrated an OFP of the Indian National Centre for Ocean Information Services (INCOIS) for coastal sea-state predictions in areas relevant to the marine industry, based on WAVEWATCH-III and SWAN models. Bonino et al. [31] presented a pilot WFS in the Northern Tyrrhenian and Ligurian Seas, aiming at real-time predictions around the main ports of the study area based on the MIKE21 phase-averaged Spectral Wave (SW) model with medium-range resolution. In the North Sea, researchers have presented validation of a wave analysis system using data assimilation and mesoscale model forcing winds within an integrated operational wave and sea-level forecast

platform, based on coupled SWAN-DCSM (Dutch Continental Shelf Model with flexible mesh) simulations [32,33].

Existing, freely available, oceanographic OFPs regularly refer to open-sea environments on global or regional scales, extended to dynamically downscaled applications in the coastal zone. However, most of them do not provide the required resolution in harbored nearshore areas to sustain reliable marine weather predictions (MWPs) that can increase the safety of port navigation [7]. For example, the Mediterranean component of the Copernicus Marine Service (CMS) [34,35] concentrates on the fit-for-purpose “downstream” provision of open-access large-scale environmental information to society bridging science-policy gaps, however, we want to focus on a fast-track service for real-time operational management of safe navigation in ports targeted at the maritime transport industry.

A three-level nested forecasting system in the Mediterranean Sea (focusing on the Aegean Sea and Thermaikos Gulf) with progressively downscaled wave and storm surge simulations is the WaveForUs OFP [36–38]. The used model is WAVEWATCH-III with a resolution barely reaching down to  $dx = 250$  m. The Coastal Observing System for Northern and Arctic Seas (COSYNA) [39] is an OFP with a focus on the German Bight, the North Sea, and Svalbard. The SAMOA (Sistema de Apoyo Meteorológico y Oceanográfico de la Autoridad Portuaria) initiative is focused on the needs of the port sector regarding forecasts of wind, waves, and sea level [40,41]. The produced, user-customized OFP serves the Spanish Port Authorities (Puertos del Estado) in dealing with issues of navigation safety, environmental management of harbored areas, and port-operation decision-making [42]. The SOCIB platform [43,44] is also a port sector-related product providing services on regional and local scales [45], supporting free sharing of MWPs’ data produced by an OFP for waves with a rather crude resolution of  $dx > 0.5$  km. Campos et al. [46] have developed an operational WFS in the South Atlantic Ocean using the WAVEWATCH-III model with quite high skill scores, yet a too coarse grid for the needs of port areas.

Sotillo et al. [47] have evaluated the operational CMS and the downstream services for ocean forecasting during an exceptional storm event (Gloria, January 2020) that severely affected the Spain and France coasts. The SOCIB and SAMOA (horizontal resolution of  $dx = 2$  km and  $dx = 350$  m, respectively) for coastal domains were further investigated; however, the need for near-real-time (NRT) integration of high-resolution met-ocean forecasts with local systems is underlined [48]. AQUASAFE is an OFP for marine weather predictions in several European and South American port accesses [49] to support the need for maritime productivity and safety. The downscaling level of its wave and current forecasts reaches a resolution of  $dx = 10$ – $100$  m, leading to a detailed evaluation of water depths along navigation channels. Pinheiro et al. [50] recently initiated an EWS for ship safety in Port of Sines (Portugal), called SAFEPORT, aiming at forecasting and alerting vessel operators about emergencies due to extreme weather conditions. It incorporates large-scale forecasts in the offshore area to feed wave agitation, wind, and tide simulation models based on combined SWAN/WAM spectral wave models and DREAMS [51], a linear finite element model based on the mild slope equation [52] used to simulate the propagation of monochromatic waves in port basins. These are coupled to the SWAMS package (Simulation of Wave Action on Moored Ships) [53] and BAS model [54] for the characterization of the response of a free or moored ship inside a port basin agitated by waves, winds, and currents.

### 1.3. Incentive for Proposed Application

The feasibility of maritime transports and the safety of port-related navigational processes may be undermined by severe weather conditions and consequent rough sea states or generally unfavorable sea conditions (e.g., wave periods causing resonance in ports) [55]. According to IMO [56], the determination of safe navigation routes in port areas, within the recent *e*-Navigation strategy [11], requires reliable forecasting of prevailing continental shelf, nearshore, and in-port sea states, i.e., sea level and current, wave height and period, along with wind conditions [42]. The main work frame goal is to assist in

reducing both the number and severity of weather-related maritime accidents in port areas, the majority of which involve collisions with other vessels and ship grounding on the port's seabed or on harbor structures [12,57,58]. The quality and safety of maritime transportation are, therefore, dependent on prevailing ocean and meteorological conditions in relation to the port's configuration at the time of approach (e.g., inducing excessive wave reflection, undue wave diffraction, and abnormal resonance). Key performance indicators for port management and shipping fleet routing [14] are the marine weather conditions (wave and wind characteristics) during port calls (weather routing), allowing for reliable estimation of vessel movements and turnaround times (Review of Maritime Transport) [6].

Expanding our former pilot work in the Mediterranean Sea [18], in this paper we seek to investigate the impact of sea conditions regarding an OFP for the prediction of detailed wave fields in and around very important ports throughout the globe. This application is developed in the framework of the research project Accu-Waves [15,59] which involves the implementation of operational marine forecast systems to support safer navigation in major ports worldwide. Accu-Waves aspires to assist in the time reduction in vessel transit, the enhancement of port traffic management, and freight throughput while decreasing possible operational and navigational expenses. The delivery of near-future marine conditions' predictions to all vessel operatives [60] during their approach to ports through a user-friendly web-GIS EWS [16] is an innovative, broad-scale product that can significantly increase navigational safety. It reflects the needs of target groups, such as port traffic headquarters, navigators, towage servicers, shipping companies and owners, harbor masters, ship pilots, captains, seafarer staff, fishermen, coastguards, diving technicians, etc., for seakeeping in navigation pathways, port entrances, and basins. The choice of studied ports within the proposed OFP is based on their traffic loads and the high significance of maritime transport services, based on the ever-growing datasets of MarineTraffic [61].

Any Decision Support Tool (DST) for safe navigation in and around ports that aspires to be robust should be based on reliable WFS products (3 days in advance) and a user-friendly OFP for port navigation control and operational managers, ship masters and vessel captains, pilotage support, and towage services. Therefore, Accu-Waves aims at the following:

1. uninterrupted computational performance of all the OFP subsystems,
2. perpetual hardware operations for data preparation, hard-disk storage, and code executions,
3. unhindered communication with external sources of large-scale met-ocean forecasts,
4. nonstop operability of conditionally sequenced numerical modelling components,
5. continuous data-streaming and interaction of produced results,
6. securing forecast conclusion and dissemination against contingencies, and the transferability of high-focus WFS to end-users via an easy-to-use web-GIS app.

#### 1.4. Article's Structure

Following the introductory section, Section 2 describes the modelling and computational methods implemented in the OFP, the created topographic and bathymetric information, and the available observational field data used in this study for model validation. Section 3 presents the setup of the Accu-Waves forecast system with its architecture, the features, and the inner-workings of the OFP with its software execution sequence. Section 4 presents the evaluation of the wave models based on the use of field measurements and comparisons with another established OFP. The results of the forecast model operation are also analyzed for both usual sea-states and exceptional storm wave conditions. Several operational issues are discussed in Section 5. The main concluding remarks are presented in Section 6.

## 2. Methodology and Datasets

In all the above-mentioned efforts, the study areas are generally much wider than the typical domains around the ports that we present herein. Therefore, inevitably, the finest

grid resolution of the usually implemented 3rd generation phase-averaged wave models in typical OFPs is coarser than the characteristic dimension of the largest mesh elements in our spectral wave model simulations (see Section 2.3). Moreover, there is a need for phase-resolving model implementation in order to simulate the detailed wave propagation near harbored coastal areas and the wave penetration and agitation in ports, diffraction due to jetties and breakwaters, and reflection from piers and waterfronts [62]. Hence, we hereby also incorporate a phase-resolving Hyperbolic Mild-Slope (HMS) equation model with high-order spatial discretization ( $dx \leq 3.5$  m) near and inside port basins (Model B; see Section 2.2), coupled to very fine spectral wave modelling ( $dx \geq 50$  m) in nearshore areas around ports (Model A; see Section 2.2). The coupled wave models are fed with reliable model forecasts (combining tide- and weather-induced circulation) for sea level elevation and depth-averaged currents in coastal areas [63] (Model H; see Section 2.4). The research output combines information about marine weather conditions that can decisively influence port operations and maritime transport (ship maneuvering and towing, vessel docking, etc.). These also include the respective wind conditions (velocity and direction), which are crucial to the aforementioned processes. The daily delivery of comprehensive and detailed WFS data to navigational traffic control and vessel operatives through a user-friendly OFP is a novel endeavor towards the enhancement of navigation safety in big cargo ports with high traffic loads [15,17,64]. The produced web-GIS app of our OFP operates in 50 selected important ports worldwide in support of port approaching procedures for any type of vessel calling at harbor facilities. It offers reliable wave and sea conditions' data on interactive GIS maps of prevailing 3-hourly sea-states in and around port basins for a 3-day forecast updated every day. Figure 1 presents the main ship traffic lanes, depicting the annual density of cargo vessels transiting among the major ports in all referenced seas of the global ocean, including all the studied ports herein.

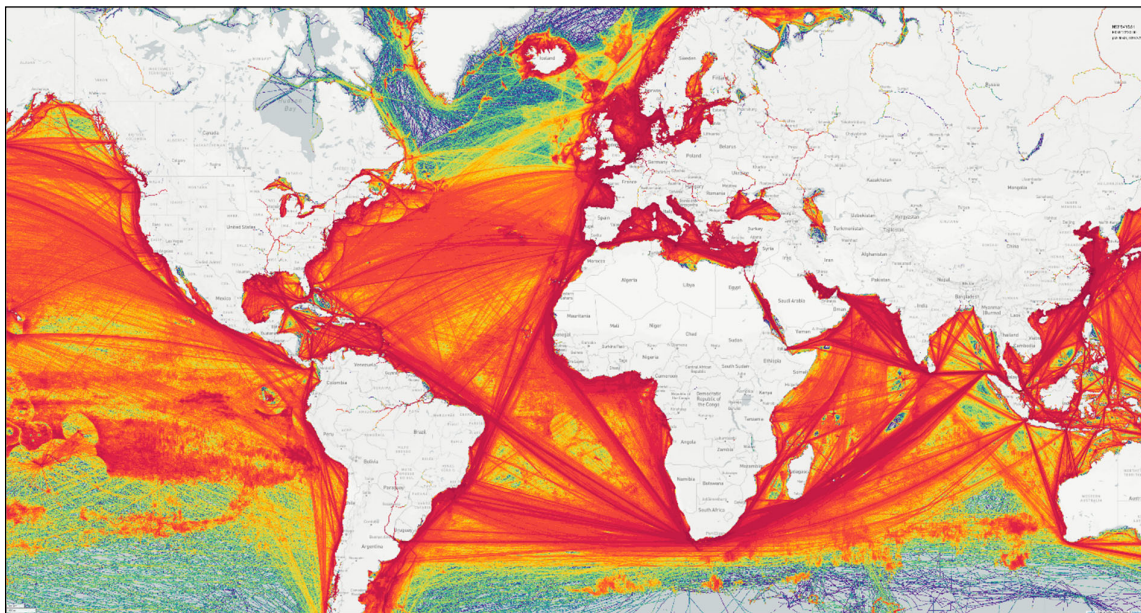


**Figure 1.** Depiction of the main ship traffic lanes and navigation routes transiting among the major ports in the global ocean; colour bar represents the annual density of cargo vessels, based on Automatic Identification System (AIS) datasets for the year 2020; Courtesy of MarineTraffic—Global Ship Tracking Intelligence [61].

### 2.1. Case Study Areas

The main selection criteria of the case study port areas within the proposed Accu-Waves OFP comprise their commercial importance and high significance of maritime transport services, their shipping traffic load, and the global navigational correspondence

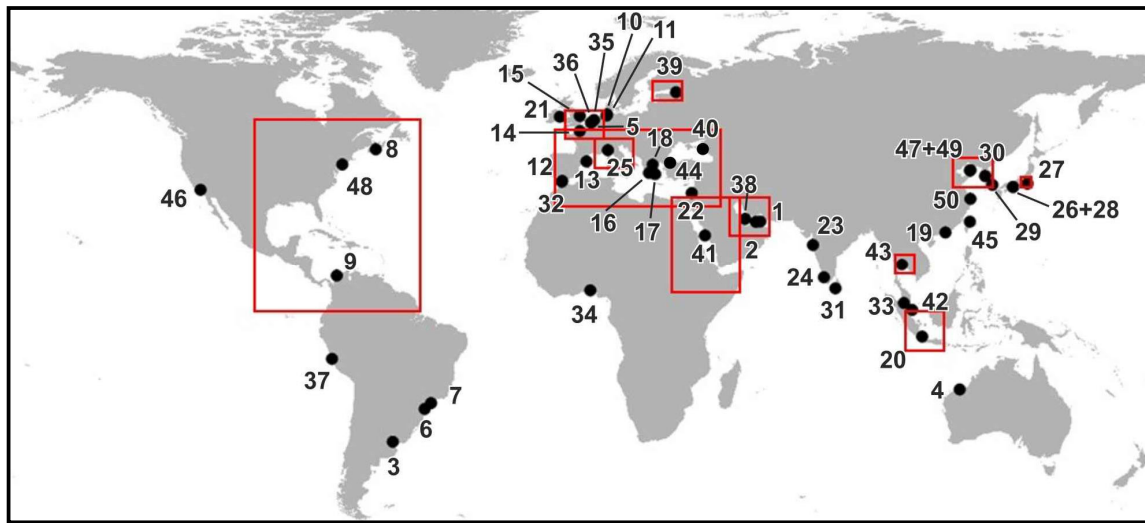
of port-visiting vessels (Figure 1) [65]. These refer to almost all large ship types, such as bulk (cargo) carriers, container ships, cruisers, ocean liners, roll-on/roll-off (ro/ro) vessels, tankers, etc. Our perspective was that at least one representative vessel per aforementioned category of ships is visiting the chosen ports on a recurring (minimum weekly or monthly) schedule in order for a port to be included in our OFF. Details on a maritime network analysis, based on connectivity and spatial distribution of port locations and inter-port shipping flows, can be found in [65] for the European maritime grid until 2017 (up-to-date datasets for the start of Accu-Waves in 2018 were available to the project’s members). The list of 50 ports selected for the Accu-Waves application is provided in Table 1. We further opted to choose characteristic coastal areas and large marine aquatic bodies evenly spread out all over the globe; the harbor sites are depicted in Figure 2 together with the surrounding areas of the supporting sea level prediction model implementation on a global map.

**Table 1.** List of selected ports for Accu-Waves OFF.

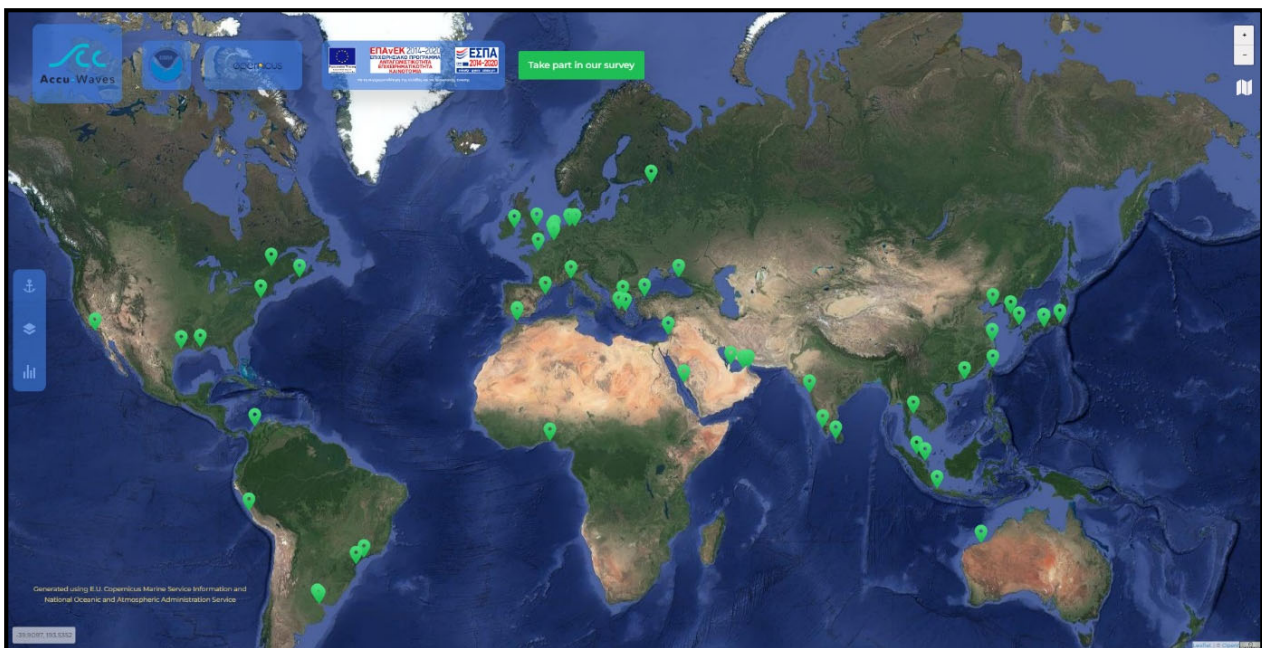
A/A.	Port Name	Country	Lat, Lon (°)	A/A	Port Name	Country	Lat, Lon (°)
1 *	Fujairah	UAE	25.18449, 56.376976	26	Osaka	Japan	34.481998, 135.215596
2	Jebel Ali	UAE	25.115958, 54.992612	27	Tokyo	Japan	35.358128, 139.721075
3 *	Buenos Aires	Argentina	−34.408068, −58.217592	28	Kobe	Japan	34.481998, 135.215596
4	Port Hedland	Australia	−20.295223, 118.579852	29 *	Busan	Republic of Korea	35.040455, 128.777307
5	Antwerp	Belgium	51.761809, 3.584792	30	Incheon	Republic of Korea	37.382372, 126.518003
6	Paranagua	Brazil	−25.553207, −48.268124	31 *	Colombo	Sri Lanka	6.958612, 79.819435
7	Santos	Brazil	−23.983137, −46.286548	32 *	Tanger Med	Morocco	35.896937, −5.531744
8 *	Halifax	Canada	44.589519, −63.521229	33	Klang	Malaysia	3.017965, 101.172777
9 *	Cartagena	Colombia	10.4012, −75.684413	34	Lagos	Nigeria	6.423271, 3.378338
10	Bremerhaven	Germany	53.634542, 8.432954	35 *	Ijmuiden	Holland	52.470833, 4.52835
11	Hamburg	Germany	53.970308, 8.598527	36	Rotterdam	Holland	51.998589, 3.980189
12 *	Algeciras	Spain	36.103713, −5.376105	37 *	Callao	Peru	−12.040148, −77.178332
13 *	Barcelona	Spain	41.323029, 2.197049	38	Ras Laffan	Qatar	25.916437, 51.694296
14 *	Le Havre	France	49.486063, 0.06775	39 **	St Petersburg	Russia	59.923369, 30.121587
15	Immingham	UK	53.554267, 0.107858	40 *	Novorossiysk	Russia	44.655115, 37.824991
16 *	Patra	Greece	38.251791, 21.690261	41 *	Jeddah	Saudi Arabia	21.455015, 39.127487
17 *	Piraeus	Greece	37.929029, 23.587359	42	Singapore	Singapore	1.160392, 103.747156
18 *	Thessaloniki	Greece	40.448321, 22.829513	43	Bangkok	Thailand	13.492719, 100.593242
19	Hong Kong	China	22.248463, 114.133737	44 *	Ambarli	Turkey	40.949147, 28.676802
20	Jakarta	Indonesia	−6.041035, 106.859654	45 *	Keelung	Taiwan	25.163773, 121.762476
21 *	Dublin	Ireland	53.333206, −6.10403	46	Los Angeles	USA	33.715401, −118.188251
22 *	Haifa	Israel	32.854963, 35.00941	47	Dalian (Dayao)	China	38.990992, 121.931578
23	Mumbai	India	18.888354, 72.824252	48	New York	USA	40.517758, −73.951194
24	Cochin	India	9.95638, 76.225454	49	Dalian (Bay)	China	38.921425, 121.748244
25 *	Genova	Italy	44.364064, 8.857234	50	Shanghai	China	31.288889, 121.927287

\* Ports where both A and B wave models are applied. \*\* Under (re)construction due to a lack of free bathymetric data.

The bathymetric grids, created for the models’ implementation, were built in a meticulous way to contain very detailed topographical characteristics of the sea bottom and the shoreline in the areas of all the selected port sites (Table 1, Figure 3). For the sake of brevity, topographic extents and/or bathymetric maps of all ports are provided in the Supplementary Material (no. S1, S3, and S4), next to the relevant model results; as an example, Section 4.2.2 contains the respective portrayal of the Barcelona port configuration. All unstructured meshes and structured grids of Models A and B, respectively, were based on Kriging interpolations with QGIS of digitized scattered data acquired by available nautical maps of the National Hydrographic Services, e.g., Hellenic Navy Hydrographic Service (HNHS) [66], EMODnet bathymetries [67], and the detailed charts of the Navionics platform [68]. The last one also contains point depictions and high-resolution contours from sonar bathymetric charts. The large-scale georeferenced data of the latest General Bathymetric Chart of the Oceans (GEBCO) [69] database was further used to build the staggered bathymetric grids of Model H (see Section 2.4 and Figure 3a for respective area extents).



(a)



(b)

**Figure 2.** (a) Depiction of the selected 50 ports’ locations (black dots) for Accu-Waves OFP around the world; red rectangles demarcate the large areas of sea level and current predictions with our supporting storm surge model (see Section 2.4); numbers correspond to the list in Table 1. The ports that are not included in the red areas receive sea level and current forecast input from CMS. (b) Depiction of the Accu-Waves OFP web-GIS app [70], including more ports, e.g., Houston and New Orleans in the Gulf of Mexico, etc., intended for the expansion of the Accu-Waves WFS network.



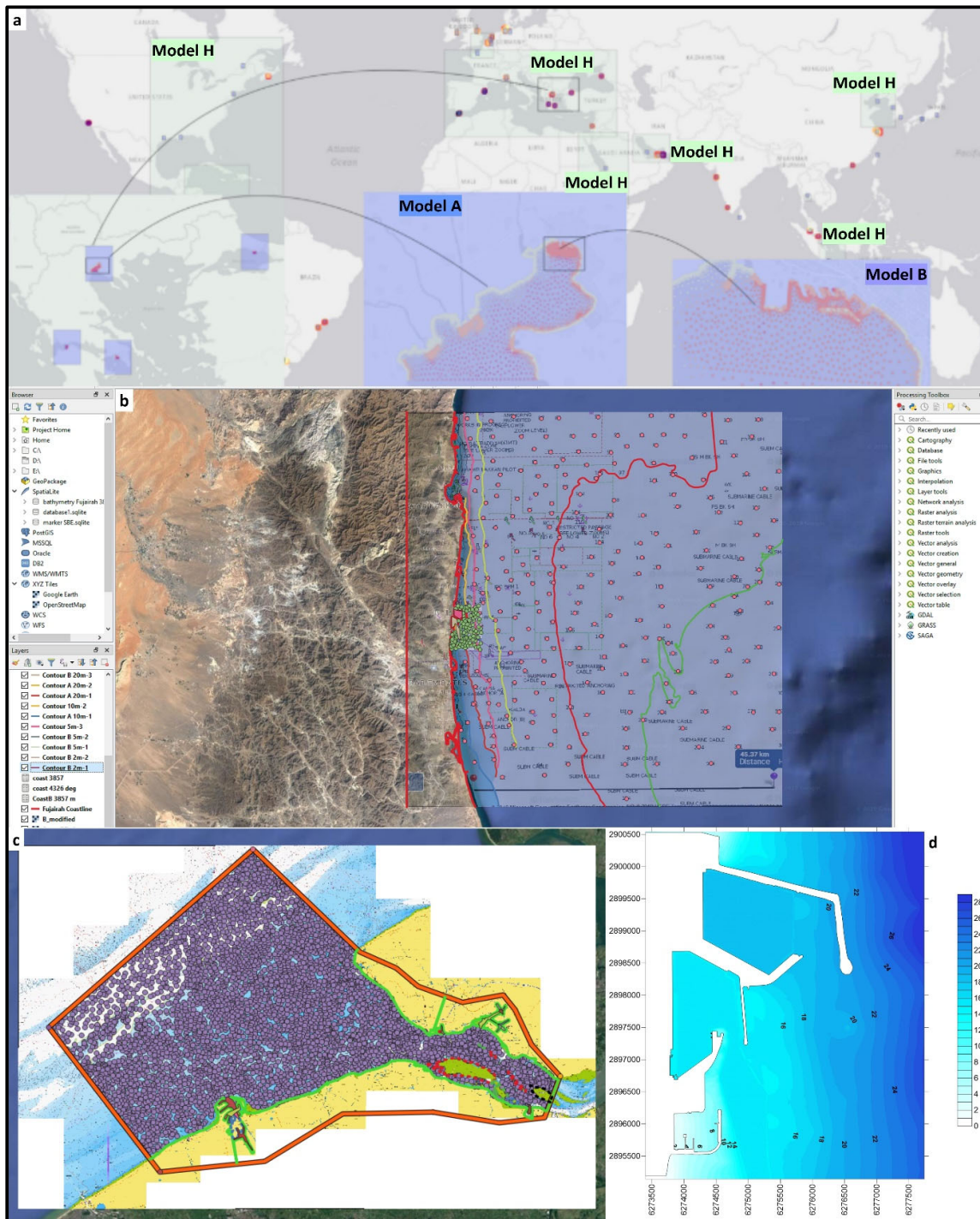


**Figure 3.** Depiction of the digitization processing of bathymetric data for selected port locations. (a) Global chart with 50 important ports from Table 1 (marked with dots); green hatched areas correspond to Model H domains; zoomed panels refer to Model A and B domains in the Thermaikos Gulf and port of Thessaloniki (Greece; port no. 18) for Accu-Waves OFF. (b) QGIS processing of recorded depth contours and measured points by local nautical charts down to a scale of 1:5000 (here Fujairah; port no. 1). (c) Densification of digitized bathymetries by Navionics free sonar/point chart data. (d) Final interpolated bathymetry, Depth  $d$  (m), in a typical port configuration containing all coastline and waterfront details, convex seafront formations, diverse bed topography, etc. (Fujairah port).

Model A implementations cover simulation domains on the continental shelf with areas of 45 km radius from each of the 50 ports' centers (Table 1; see topographic ex-

tents and/or bathymetric maps of all ports in Supplementary Materials S1, S3, S4, and Section 4.2.2 for Barcelona port). A coastal area extent of nearly 25 nautical miles along the port approach should practically capture the local wind effects (coastal area fetch) on wave generation and/or amplification in gulfs and bay areas [15]. Model B is currently applied by one-way coupling to Model A for almost half of the selected ports (i.e., those with such simulation domain extents allowing for reasonable computational requirements). Model B runs only inside harbored areas, and its configuration contains all the shoreline and bathymetry details of natural or built waterfronts and port approaches, respectively (Figure 3d). In open ports (i.e., with no entrance, only protective detached breakwaters), it runs on a domain where the open-boundary wave generator is several wavelengths away from the reflective windward side of the main breakwater. The two models are nested by choosing the most homogenous wave generation line for Model B in terms of water depth (Figure 3a). In ports where Model B is not applied yet, Model A simulates wave fields inside port domains using highly densified digitized bathymetric data (Figure 3c), reaching a resolution of a few tens of meters in the nearshore areas of the port basin.

The input of sea level and currents' predictions is derived from Model H applications [18,71] in broader domains than those of the wave simulations. These cover oceanic areas, marginal seas, and large gulfs in order to pertain the synoptic-scale meteorological effects on modelled sea level variations, especially for severe weather conditions (storms, hurricanes, typhoons, etc. [72–75]). These aquatic bodies include the north-western part of the Atlantic Ocean, the Mediterranean, Java, Black, Red, and Yellow Seas, the English Channel, and the Finland, Osaka, Persian, and Tokyo Gulfs (Figures 2a and 3a).

## 2.2. Wave Models

The prototype model suite comprises tested solvers, i.e., a high-resolution spectral wave model [76,77] and a nested fine-resolution HMS wave model [78,79], referred to as Models A and B. These are fed by the outputs (sea level and current forecasts) of a barotropic hydrodynamic circulation simulator (Model H) [18,71]. Their operational mode is controlled via *Python* codes and *Dask* library, designed for automation of simulations in all ports. The latter are executed in parallel for optimal delivery of the high-end wave modules' outputs on time every day [17]. Thus, we hereby also present the end-to-end computational processing route of the integrated WFS model suite (see Section 3). It is created to manage (i.e., retrieve, translate, handle, fuse, simulate, integrate, post-process, validate, and visualize) georeferenced numerical big data (daily storage volumes:  $O(100)$  GB; daily produced volumes:  $O(1-10)$  TB). We also provide the OFP models' verification and visual representations of characteristic model applications during their evaluation phase (see Section 4). The related sea conditions refer to the following parameters:

- (a) weather data: wind speed and direction (for wave forecast models), and sea level pressure (for the supporting sea level prediction model);
- (b) wind-induced spectral wave characteristics (significant wave height, spectral peak period, and main direction of wind wave propagation) in the entire coastal area where the studied port is located;
- (c) offshore swell characteristics (height, mean period, and main direction of long oceanic waves) by the inclusion of a simulation of the double-peak spectrum in the spectral wave model, including wind sea and swell sea data on the open boundary with the open sea;
- (d) very detailed propagating pseudo-spectral wave parameters (wave height, period, and main direction of propagation) inside the port basins;
- (e) possible reflecting wave patterns and standing wave (seiche) depictions in the port basins;
- (f) accompanying information about sea level elevation due to meteorological conditions and tidal effects and the respective barotropic ocean currents' velocity/direction.

Model A is based on a TOMAWAC [80] implementation. It is a 3rd generation (phase-averaged), spectral (frequency and directional,  $f-\theta$ , formulated), wave action model that can simulate the generation and propagation of wind-induced irregular waves on triangular

finite element meshes [81]. Model A considers irregular wave shoaling, white-capping and depth-limited breaking, energy dissipation due to bottom friction, non-linear triad and quadruple wave-wave interactions, and a rudimentary approach for wave-structure interaction (e.g., diffraction). The Model A domain resolution is densified as waves propagate over shallower waters in the coastal zone and near ports, reaching down to a typical spatial discretization of 50 m [18,76]. Model A can also capture the wave-current interactions [77]. Model H output due to wind-, tide-, and surge-induced barotropic hydrodynamics and sea level is set to automatically update the input of water level, currents' speed, and direction in 3-hourly intervals. Thus, within this Model H to A configuration about hydrodynamic current coupling, Model A simulations can capture more reliable estimations of the mean spectral wave and swell directions for sea conditions agitating the selected ports.

Model B is based on WAVE-L, an HMS equation [82] simulator developed by members of the author team (from Aristotle University of Thessaloniki) for the propagation of non-linear monochromatic waves over a rapidly changing, uneven seabed [83]. It incorporates shoaling, refraction, diffraction, (partial and total) reflection from (sloping and vertical) structures [84], energy dissipation due to combined wave breaking [85], and bottom friction [78,86,87]. Makris et al. [18,79] have analytically presented the latest versions of the model that treat quasi-irregular wave generation and propagation [88,89] with any incident wave direction following the manipulation of lateral boundaries by Lee and Suh [90], based on Vincent and Briggs [91]. Furthermore, Model B applies a protection against numerical contamination of its domain by the peripheral sponge layer treatment [92]. The implemented rectangular grids are of very fine resolution,  $dx \geq 2$  m. The numerical solution algorithm follows a quick explicit scheme [93] to account for very demanding simulations incorporating staggered grids of up to 8–10 million cells. Table 2 presents all the basic information about the parameterizations and attributes of wave models A and B.

**Table 2.** Basic parameterizations and attributes of the wave models (A and B).

Attribute	Name/Parameterization	Implementation/Configuration Characteristics
Wave model	TOMAWAC (Model A)	3rd generation phase-averaged spectral
Area of application	Gulfs, Bays, and Coastal Seas	e.g., Thermaikos and Tokyo Gulfs, Iberian and Red Sea, etc.
Domain dimension	Port approaches, including anchorages	Radius of 45 km from the port center
Forcing/Driving field	NOAA	$W_x$ and $W_y$ products, $0.1^\circ \times 0.1^\circ$ , 3 h
Initial/Boundary conditions	CMEMS Copernicus	MEDSEA ANALYSIS FORECAST WAV-006-017 products $0.042^\circ \times 0.042^\circ$ , 1 h
Spatial resolution	Varying domain	Finite Element of typical dimension $dx = 50\text{--}500$ m
Bathymetry	Regional hydrographic services	Local nautical map digitization (Navionics, etc.)
Frequency range	0.04–1 Hz	Typical wave periods: $T_p = 1\text{--}25$ s
Integration time step	$\Delta t = 10$ min	Output every 3 h
Integration scheme	MoC for propagation	Semi-Implicit for source terms
Wave model	WAVE-L (Model B)	Hyperbolic mild-slope equation phase-resolving
Area of application	Port basins	e.g., Algeciras, Busan, Colombo, Halifax, Jeddah, Patra, etc.
Domain dimension	From port entrance to waterfront	Typical coastal area of $5 \times 3$ km <sup>2</sup> in and around ports
Driving field	Model A results	$H_s$ , $T_p$ , $a_p$
Spatial resolution	Fixed rectangular grid domain	$dx = 2.5$ m in port approaches and harbor basins
Bathymetry	Regional hydrographic services	Local nautical maps digitization (Navionics, etc.)
Integration time step	$\Delta t = 0.1$ s	Output every 3 h
Wave-breaking model	Eddy viscosity concept	Battjes and Janssen [85]
Boundary conditions	Peripheral sponge layer	Partial/Full reflection [84]
Wave generation	Quasi-irregular waves	Lee and Suh [90]

The partial wave reflection regime from port structures is numerically approximated by a semi-explicit scheme of calculation via a system of complex number equations [84] for the horizontal eddy viscosity. The reflection coefficient from, e.g., rubble mound breakwaters is pre-estimated based on classic empirical relations in the literature [94]. Therefore, a very meticulous recording of the types of solid boundaries in the selected ports followed the detailed mapping process of the numerical bathymetric grids. According to the classification of the reflection coefficient  $C_r$  of typical port and coastal structures [95], we divided all shoreline boundaries in Model B into fully or partially reflective boundaries and dissipative beaches, based on: (a)  $C_r \leq 0.15$  for natural coasts (slope < 13%); (b)  $C_r \leq 0.45$  for absorbing piers or rough armor slopes and rubble mound breakwaters (with acropods, dolos, or rocks; 13% < slope < 90%); (c)  $C_r = 0.9\text{--}1.0$  for (almost) vertical quay walls (blocks/caisson; 90% <

slope < 100%). Figure 4 presents typical examples of the classification of perimetric solid boundaries throughout the port shoreline and detached protection structures. The waterfront slopes were determined by the inspection of the latest *GoogleEarth* GIS maps; Figure 4 refers to Le Havre (France), Haifa (Israel), and Genova (Italy) ports (no. 14, 22, and 25 of Table 1, respectively). All the other ports were set up in the same way; more characteristic examples are provided in Supplementary Material S1.

### 2.3. Model Integration and Input by Model H

The integrated hydrodynamic (H) and wave model (A and B) application refers to one-way coupled simulations ( $H \rightarrow A \rightarrow B$ ) with a nested Model B to A domain in harbored waters, viz., near coastal works and inside port basins. Model H is based on the High-Resolution Storm Surge (HiReSS) simulator, a 2-DH numerical code for storm surges, simulating the barotropic hydrodynamic circulation and sea level variations based on the depth-averaged shallow water equations [18,71,96,97]. Its application covers regional geographic scales with a focus on the continental shelf, considering the combinatory effects of large barometric systems and wind fields, geostrophic effects (Coriolis force), seabed friction, horizontal eddy viscosity, etc. in open seas.

The model integration follows the sequence of application presented in Makris et al. [18]. Thus, Model H [71] is forced with atmospheric input (wind and Sea Level Pressure, SLP, at  $0.25^\circ$  resolution) from the Global Forecast System (GFS) [98] for weather prediction by the National Oceanic and Atmospheric Administration (NOAA) [99]. On the open boundaries of Model H, it is fed with CMS Physics Analysis and Forecast daily updated prognoses of Sea Level Elevation (SLE) and tidal currents with a resolution of  $1/12^\circ$  for global ocean products and  $0.042^\circ$  for regional scale products (e.g., in parts of the Atlantic Ocean, the Black and Mediterranean Seas, etc. [34]).

Eventually, Model H produces high-resolution three-hourly estimates of SLE and depth-averaged barotropic currents (speed and direction) due to the combined action of atmospheric conditions (wind setup and inverse barometer effect) and astronomical tides [18,72]. This way, the mean sea level and hydrodynamic flows in the Models A and B domains are updated at each timestep of implementation in a three-hourly interval for the three-day forecast. CMS forecasts of irregular wave and swell characteristics, i.e., significant wave height,  $H_s$ , peak spectral period,  $T_p$ , and mean wave train direction,  $\varphi_w$ , are provided on Model A's open-sea boundaries [100]. Almost 2/3 of the CMS input data are obtained from the global-scale Ocean Waves Analysis package ( $1/12^\circ$  resolution). The rest of the CMS datasets are retrieved from the NW European, Mediterranean, and Black Sea regional components, which are of finer resolution ( $1/24^\circ$ – $1/40^\circ$ ). NOAA wind predictions force the TOMAWAC implementations over its entire domain of application to simulate irregular wave propagation and transformation from offshore regions towards the port areas [15,17,18]. Model A runs in a mixed wind-sea/swell mode. Lastly, in the course of simulations, Model B is nested to the Model A domain in the port basin and is fed with boundary conditions of wave height, period, and direction from Model A forecasts in order to simulate the wave agitation inside the harbor basins and near their entrances or detached coastal protection structures [17,18,79].

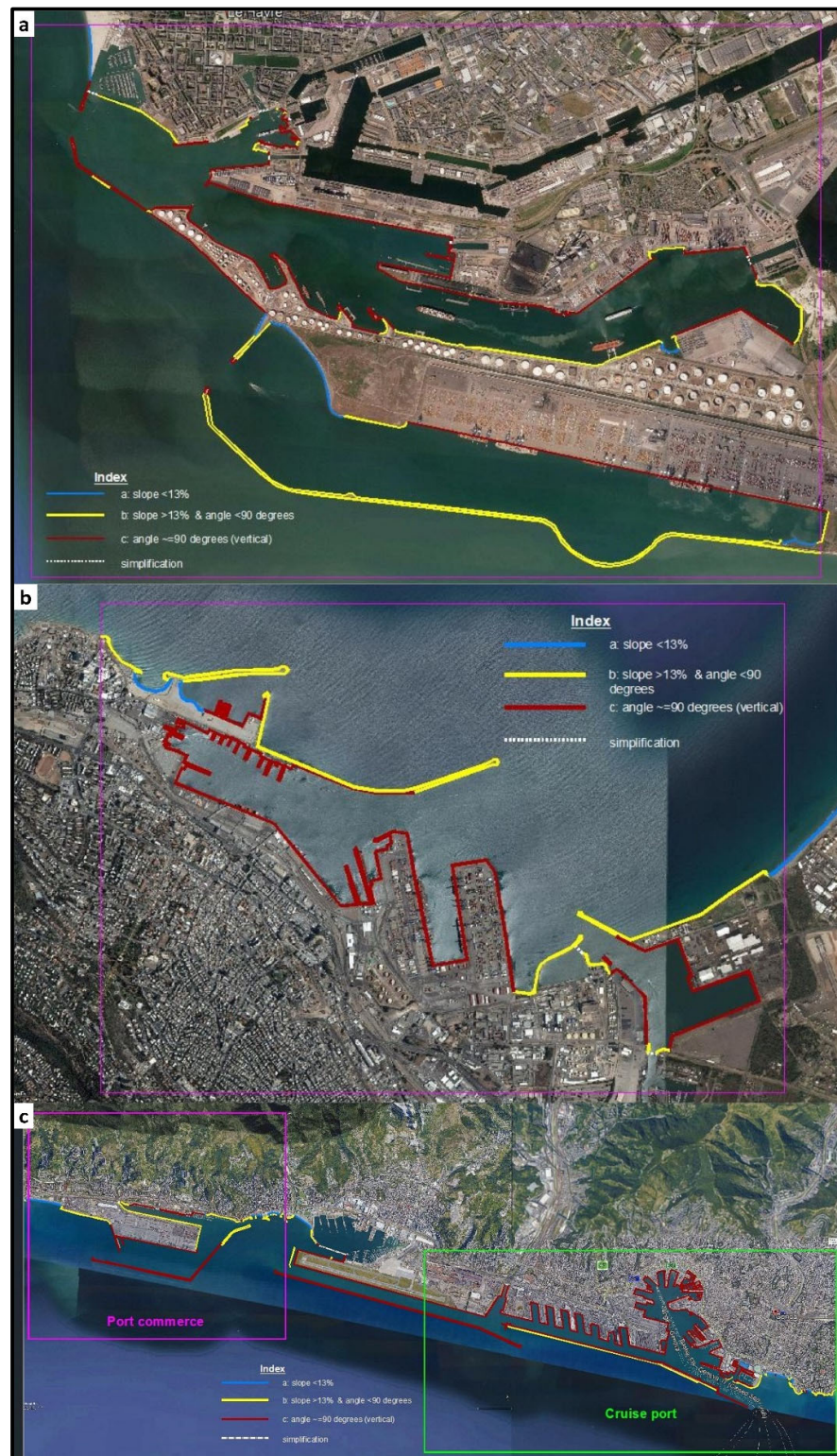


**Figure 4.** Examples of illustrative maps for the classification of the waterfront’s slope on the perimetric solid boundaries in Le Havre (**upper-**), Haifa (**middle-**), and Genova (**lower-graph**), ports no. 14, 22, and 25 of Table 1, respectively. Colors define the type of coastal seafront: (a) natural beaches (blue); (b) absorbing jetties, rough armor slopes, and rubble mound breakwaters (yellow); (c) fully reflective vertical quay walls (red). These correspond to certain values (see referred text) of the estimated wave reflection coefficient in Model B simulations.

#### 2.4. Available Data for Model Application and Validation

Makris et al. [17,18] have presented a detailed validation of all the modelling components (H, A, and B) of Accu-Waves based on comparisons against experimental and field data in the OFP's setup, hindcast, and preoperational test phase. Models H and A were validated in hindcast mode against in situ observations at several ports in the Mediterranean basin (e.g., Algeciras, Barcelona, Genova, Trieste, Venice, Alexandroupoli, Mykonos, Lefkada, Chios, Piraeus, Thessaloniki, and Haifa). Model B was validated against experimental data from classical physical simulations in 2-DH laboratory wave flumes [88,89,91]. Model B was further calibrated and evaluated against real-time field data of wave characteristics in the port of Thessaloniki during the winter period of 2019–2020.

Here, we present a verification and reliability check of our WFS (Models A and B) in its operational forecast phase against available wave data in other ports within the integrated modelling product of the Accu-Waves OFP as a quality control of its performance. The model evaluation relies on available field data on wave characteristics in and/or near ports. Modelling output from other established OFPs (e.g., Puertos del Estado) [101] has also been collected. The in situ observations and model forecasts of wave parameters from sea-surface buoys and WFS, respectively, refer to the ports of Algeciras (Spain) in the Mediterranean Sea, Antwerp (Belgium) in the North Sea, and Los Angeles (USA) in the North American coast of the Pacific Ocean (ports no. 5, 12, and 46, accordingly in Table 1). We used data-mining codes to retrieve quality-controlled, NRT, in situ observations of spectral wave characteristics from the CMS platform via the *Python-motu* client [102]. These are the Copernicus' Global Ocean In Situ Near-Real-Time Observations hourly datasets updated within 24–48 h from acquisition on average and then distributed by Copernicus 'In Situ Thematic Centre' (INSTAC) [103]. The data are wave buoy datasets from the NRT-CMS repository of observations (in  $1/30^\circ$  resolution), e.g., in the navigational approach routes of Los Angeles and Antwerp ports. For further technical details about polar coordinate positions, buoy depths, and distances from the coast, as well as download preferences, the reader is referred to the dataset [104]. Datasets are pre-tested according to the characteristics of the used equipment (default precision, calibration tactics, sampling rates, recording times, frequency of operation, etc.) by the certified global collection networks of the pre-World Meteorological Organization Global Telecommunication System (pre-WMO-GTS) [105].

Figure 5 presents the exact geolocations of the wave gauges in the ports of Antwerp-Zeebrugge (8 buoy stations) and Los Angeles (3 buoy stations) retrieved from NRT-CMS INSTAC, and model stations (numerical wave gauges) for the port of Algeciras (9 stations) provided by courtesy of the Puertos del Estado. For the needs of a NRT evaluation of the Accu-Waves WFS, we compared the available model with field data within a period of three weeks (1 May 2021 to 23 May 2021), i.e., during the hours/days that wave variables from both model predictions and corresponding in situ observations were available for each buoy station in all ports. The comparison of point-site field data with our WFS from Models A and B was performed using the nearest neighbor interpolation technique to fit the position of the corresponding model node to the specific location of the wave gauge. We further assessed the Accu-Waves WFS performance at the port of Algeciras (Spain; no. 5 in Table 1) by comparisons with an official Spanish OFP output, namely SAMOA [106], the "Local Wave Forecasting System at the Harbor Authorities" (SAPO System of Puertos del Estado), based on the WAM model [107].

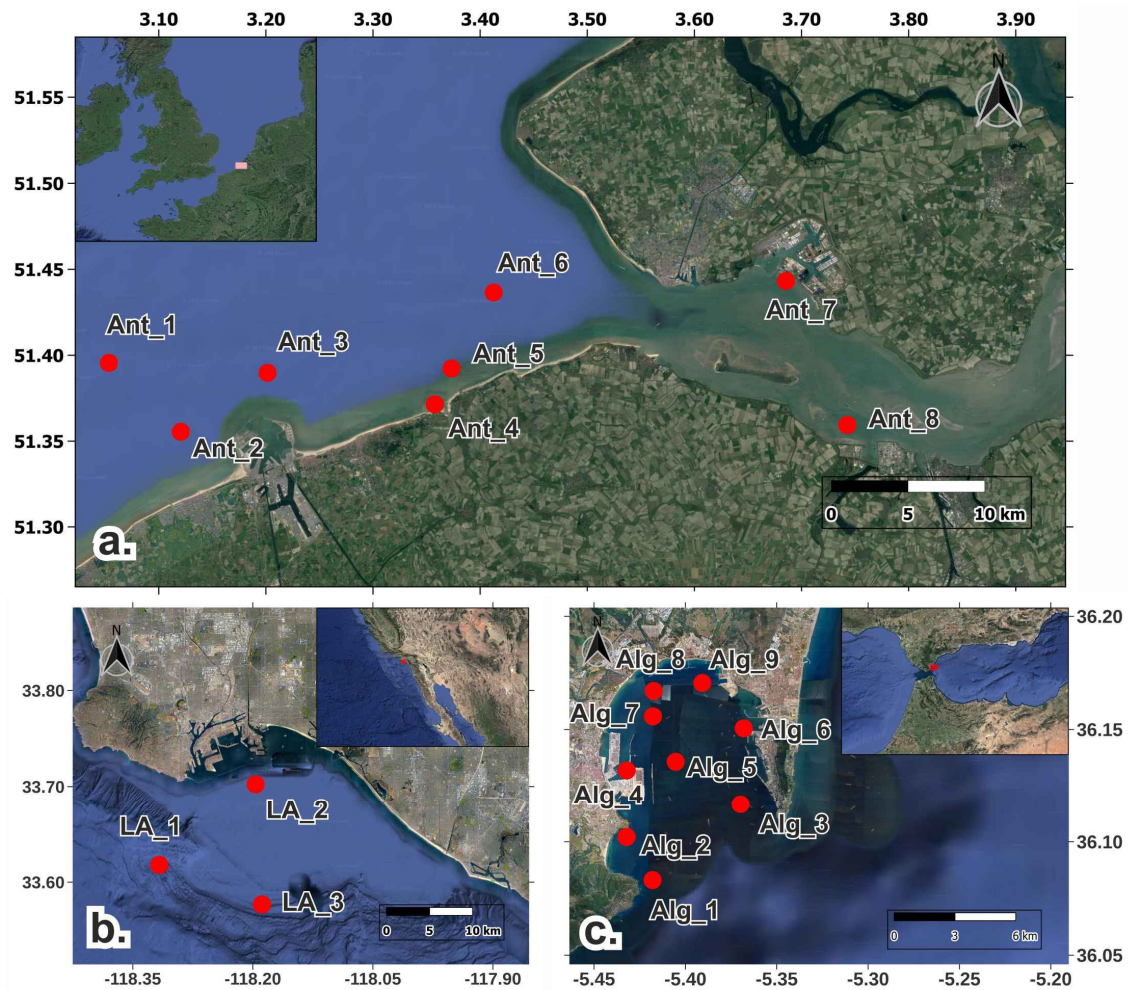


**Figure 5.** Locations of the buoy gauges that provided datasets of spectral wave characteristics in the ports of (a) Antwerp-Zeebrugge (8 stations, **upper chart**) and (b) Los Angeles (3 buoy stations, **lower left chart**) courtesy of NRT-CMS INSTAC, and (c) the port of Algeciras (9 model stations, **lower right chart**) courtesy of the Puertos del Estado, no. 5, 46, and 12 of Table 1, respectively.

### 3. Setup of Accu-Waves OFP

#### 3.1. System Architecture

The Accu-Waves OFP framework follows the data flow schematics in Figure 6. The sequence of the five discrete operational subsystems first comprises the retrieval of patrimonial datasets that refer to open access forecast input from:

- NOAA [99] (meteorological forcing) runs automatically.
- CMS [34] hydrographic boundary conditions, including tidal components of sea level and currents from Aviso+ [108], run automatically.
- GEBCO [69], national and local map agencies, e.g., HNHS [66], and Navionics [68], for all the necessary bathymetric data; non-automatic operation.

Secondly, all retrieved data are transformed into model-ready, readable formats, and the daily operational filesystem is prepared (created folder levels, etc.). Thirdly, all data are stored in a backup folder system, then catalogued and archived to be used by a contingency plan side-route of executions. Thus, data are inserted into a transformation-translation component and sent to an SQL database that supports the latter stages of the web-GIS application. These actions are all led by a series of built-in *Python* and *NumPy* scripts that allow for navigation and operation of all input and output of the model execution and the data processing components. The fourth OFP level controls the execution of all model simulations in an integrated way, based on the *Python* and *Fortran* main sets of codes within

a parallel CPU job execution [16]. The OFP systematically manages operational big data on a daily schedule. The job orchestration and parallel execution of all tasks stand on a *Python* framework relying on *Dask* [109] panel data analysis (*pandas*) workflows for automation and asynchronous operation [17]. The model forecast products are then conditionally validated against field observations, if and where available, by CMS in situ sub-datasets (2nd stage). In the fifth subsystem, all the forecast model outputs are post-processed (interpolated, filtered, combined, integrated, etc.) and then automatically visualized via *Matplotlib* codes. The final processing step formulates the platform for dissemination of operational forecasts and related data, announcements, or information towards end-users (i.e., the Accu-Waves web-GIS app) relying on *Leaflet* technologies. Characteristic details and depictions of the Accu-Waves OFP schematics of WFS model execution are provided in Supplementary Material (SM) S2 in tandem with patrimonial (external) and produced (internal) data flow.

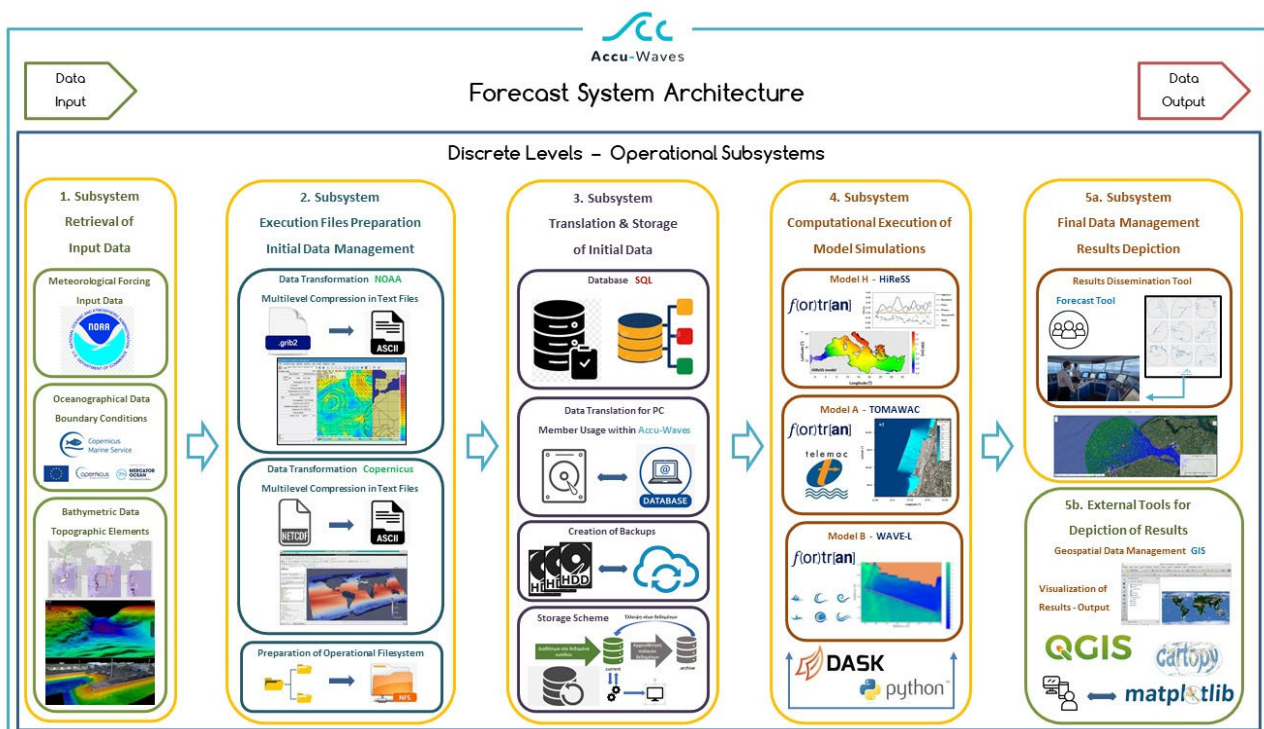


**Figure 6.** Schematics of the Accu-Waves OFP data flow depicting the sequence of several discrete levels of operational subsystems from open-access data acquisition and via model processing and validation of forecasts to final output post-processing and dissemination to end-users: 1. Retrieval of input data; 2. File preparation and initial data management; 3. Translation and storage; 4. Integrated modelling component; 5. Final results management and depiction (including web-GIS tools).

### 3.2. OFP Subsystem Features

The OFP runs on *Linux* O/S on a multi-CPU server with 128 GB of RAM and several TBs of Data Storage Units (DSUs) on Solid-State Disks (SSDs) to cope with the necessary volumes of big data created every day. Spiliopoulos et al. [17] tested its main functionalities: (a) protocols of communication and data retrieval with external sources of global-scale met-ocean forecasts; (b) software and codes for automated management and maintenance of the storage space and database regarding all the produced outputs; (c) high-resolution integrated modelling of wave propagation and hydrodynamics in regional and port scales; (d) consolidation of sea-state forecasts in 3-hourly intervals for a 3-day product visualized for the needs of port managers and navigators via tailor-made configurations.

The CPU-DSU communication operates within data transformation blocks with parallel processing in two cycles: (a) raw data storage and backup for the support of the WFS; (b) post-processing and visualization of data. This leads to the simulation and management



output of the WFS, with execution runtimes ranging from 2.5 up to 22 h depending on the needed processing power and resources, while executing ensemble simulations with the three components of the integrated modelling suite (Figure 7). To avoid data overflow of maximum storage capacity thresholds (e.g., in cases of contingency plan execution), an overall monitoring scheme of the logical procession in Accu-Waves OFP implementation is built on a coupled framework of *Python* and *Dask* [17]. The system of operations scrutinizes the availability of static (e.g., bathymetric) and dynamic (e.g., model results) data before model execution and during job orchestration in order to update the data inventory in case of contingency and alternative routes of data transfer. Therefore, the pre-defined “dossier” of port information containing georeferenced location, coastline details, upgraded local bathymetries, weather metrics, etc. is updated every day by a separate execution plan. The latter also defines the computational setups, estimates the necessary runtimes for model execution depending on data availability, sets the relevant data inflow/outflow, and formulates the interactions between all levels of implementation. Built-in *crontab* commands allow for algorithmic automation [110].

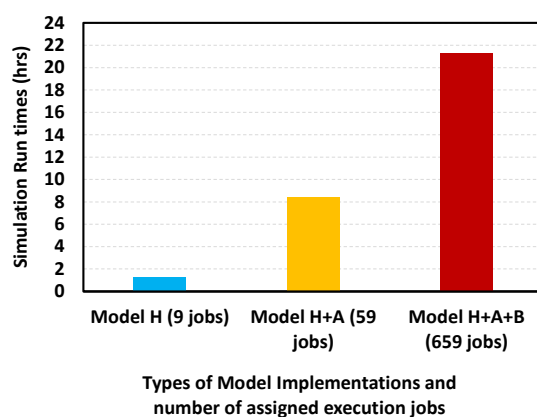


**Figure 7.** Accu-Waves WFS execution runtimes (hrs; y-axis) with ever-growing demand for processing power and resources for three discrete modelling components (x-axis): 9 Model H simulations; 9+50 Model H+A simulations; 9+50+600 Model H+A+B simulations (entire OFP modelling ensemble).

Certain operations, such as referencing, saving, routing, and exploiting all the patrimonial and produced data of the WFS, an advanced, open-source, relational database, are set up in *PostgreSQL* [16,111]. Note that input data, boundary, and initial conditions may not be available every simulation day for several ports, i.e., on certain dates, met-ocean datasets from earlier dates are utilized, thus following different file/folder routes. The latter offers constant support to the systems’ developers in delivering the forecast products and their dissemination. This way, the flowing data are stored in the Accu-Waves database, while the execution plan is saved in the filesystem for future transcriptions and easy-tracing for upcoming implementations. The OFP also pertains to code schemes for the efficient detection of severe wave agitation events in the port areas during the 3-day operational cycle. An example of the parallel execution of the Accu-Waves WFS models is further depicted in Supplementary Material S2.

Optimally, nine jobs cover the Model H simulations in 72 h forecast mode, while Model A runs in asynchronous mode with another 50 jobs for 3-day forecasts per implementation, covering the need for fine-scale spectral wave data in all the port basins and approaches. Finally, Model B theoretically needs an ensemble of 22–25 ports  $\times$  24 individual 3 h sea-states that may reach a total of 528–600 parallel jobs. This is imperative due to the nature of HMS-type models that aim at steady-state conditions per 3 h simulation of the nearshore wave regime. Conclusively, for a 3-day forecast, more than 600 jobs may be called for, also considering the intermediate communications. Note that the forecast products are automatically renewed every day to achieve a better representation of wave characteristics for at least 24 h ahead, since the farther in the timeframe of predictions one seeks, the

lower the forecast quality gets. Thus, the OFP might produce a raw total output of O (100) GB daily within the operational execution pipeline. Our *Dask* application programming interface (API) can achieve multi-core speed-up during the scheduling, communicating, and pre- and post-processing phases of model data, while maximum *Fortran* optimization compiling secures the quickest possible performance of model simulations. Hence, the Accu-Waves system consists of a novel large-scale set of macro-implementations that demand upscaled constant data flow and web interactions with cloud services for big data exchange [17]. The descriptive schematics of the Accu-Waves OFP integration execution course and interaction of the WFS model data, including all feeding parameters, are provided in Supplementary Material S2.

#### 4. Results of Model Validation and Operation

In this section, we present a basic validation of operational forecasts with models A and B in selected ports and further provide characteristic results and visual output of the OFP during moderate and rough sea conditions. The ability of our WFS to reproduce the extremely high sea conditions during a storm event in the Western Mediterranean is also investigated.

##### 4.1. Model Validation

Following our previous work on model validation [17,18] against field observations in Mediterranean ports (Models A and H) and experimental data (Model B), we expand our evaluation of the Accu-Waves OFP to other ports. Model validation was separated into two phases: (a) the setup-operational stage with multi-parametric validation per model setup, and (b) the scenario-operational stage with testing for standalone models and qualitative critique of the WFS results. In the following, we present a quality assessment of the OFP products against recorded wave buoy data and WFS model output by other established OFPs in Antwerp—Los Angeles and Algeciras ports, respectively. The duration of the implemented time series (23 days) is considered sufficient to evaluate the performance of the forecasting tool by correlating the results of simulation models against field observations. The WFS model performs better for the forecast of significant wave height,  $H_{m0}$ , than for the peak period,  $T_p$ , of the wave energy spectrum in all ports, as expected.

##### 4.1.1. Model A vs. Field Data

Model A (TOMAWAC) is a well-established, advanced, 3rd generation spectral wave model specifically designed to tackle the wind-induced generation and transformation of irregular waves in coastal zones. It has been validated by comparisons with experimental data and further tested several times in real-life problems [112]. Within the Accu-Waves initiative, we have parametrized Model A and evaluated its ability to capture spectral wave transmission, refraction, and breaking due to strong opposing currents [76,77]. These are an extra feature that can increase the reliability of wave model predictions supporting safe navigation near ports (i.e., in an area of 45 Km radius from the main port in our cases). Table 3 and Figure 8 summarize the model validation against field observations based on scatterplots and a variety of statistical measures (see definitions in Appendix A), i.e., Percent Errors, PE (%), for maxima, means, and standard deviations; Root-Mean-Square-Error, RMSE; Pearson Correlation coefficient,  $R_p$ ; Willmott Skill Score (or Index of Agreement), WSS; Hit-Rate-of-Percentiles, HRP index. These refer to the timeseries of available basic wave parameters, viz., significant wave height,  $H_s$  or  $H_{m0}$ , and peak spectral period,  $T_p$ , at the ports of Antwerp and Los Angeles (Section 2.4).

**Table 3.** Validation of models (mod) against field observations (obs) based on statistical measures: Percent Errors, PE (%), for maxima, means, and standard deviations, RMSE (m or sec),  $R_p$ , WSS, and HRP-index for the timeseries of wave parameters A: significant wave height,  $H_s$  or  $H_{mo}$ , and peak spectral period,  $T_p$ . Ports: Antwerp and Los Angeles.

Port	A: Wave Parameter	PE (%) Max $A_{mod-obs}$	PE (%) Mean $A_{mod-obs}$	PE (%) $\sigma_{A,mod-obs}$	RMSE (m or sec)	RMSE/ $A_{obs,max}$	$R_p$	WSS	HRP-Index
Los Angeles	$H_{mo}$	4.80%	5.50%	3.10%	0.136	5.90%	0.91	0.95	1.00
	$T_p$	17.1%	3.40%	19.4%	3.31	15.0%	0.31	0.60	0.97
Antwerp	$H_{mo}$	12.4%	19.4%	3.90%	0.197	7.80%	0.90	0.94	1.00
	$T_p$	18.5%	14.4%	36.8%	2.58	21.5%	0.30	0.57	0.97

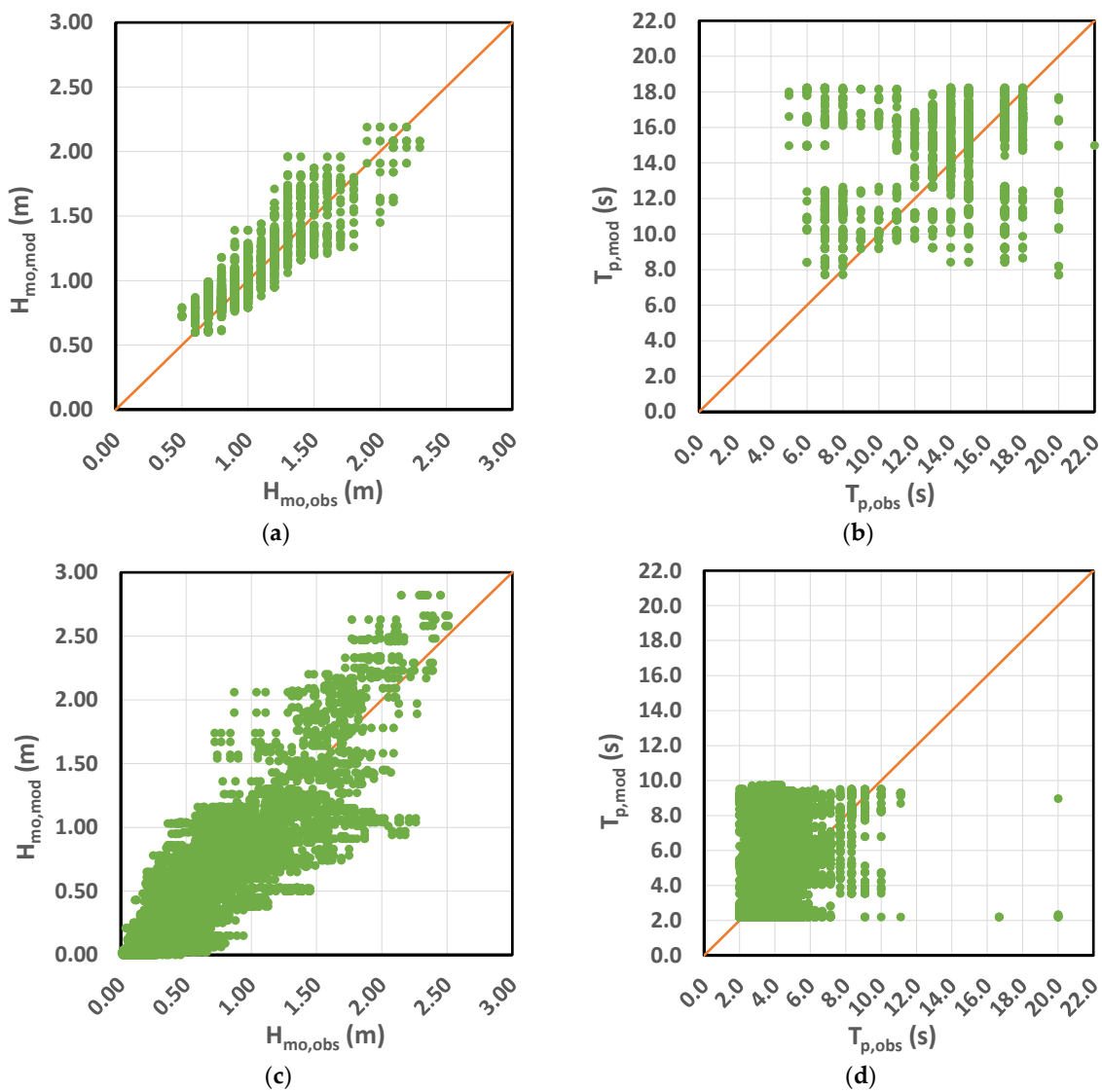


**Figure 8.** Correlation of Model A (mod) and wave-buoy field observation (obs) data by scatterplots of (a,c) significant wave height  $H_{mo}$  (left panels) and (b,d) peak spectral period  $T_p$  (right panels) values for (a,b) Los Angeles (upper plots) and (c,d) Antwerp (lower plots).

Comparisons at the port of Los Angeles range from marginal or acceptable to quite good for  $T_p$  and  $H_{mo}$ , respectively (Table 3; see Appendix A for explanation of grading). The model skill scores and correlations between model results and field data have particularly high values ( $R_p$  and WSS > 0.9 and HRP-index > 0.99) for the operational forecast of  $H_{mo}$  (Table 3). The error values (PE and RMSE) are very low, and their percentages relative to

characteristic observation maxima are particularly low, e.g., <10% for all statistical measures and conditionally <5%. The scatterplot for the correlation of simulation and observation results is clearly favorable for the WFS (Figure 8a), considering that we only have three comparison points available. The comparisons for  $T_p$  can also be considered acceptable, although less robust than for  $H_{mo}$  (e.g.,  $R_p < 0.5$ , yet  $WSS > 0.6$  and  $HRP\text{-index} > 0.95$ ). The  $T_p$ -related error values (PE and RMSE) are also quite low, and their percentages relative to characteristic observation maxima are satisfactorily lower than 20% for all statistical measures and <5% for the average values of recorded  $T_p$ .

The comparisons, based on  $H_{mo}$ , in the port of Antwerp, although slightly worse than in Los Angeles, also range from very good to exceptional. Model skill scores and correlation indices also remain particularly high for WFS models ( $R_p$  and  $WSS > 0.9$  and  $HRP\text{-index} > 0.99$ ; Table 3). Percentage errors are considered to be small, <20%, with an RMSE lower than 8% of the critical maximum magnitude of  $H_{mo}$ . Especially for  $T_p$ , there is a general deviation of the modelled timeseries from the observed datasets, but  $WSS > 0.67$  and  $HRP\text{-index} > 0.97$  (Table 3) are acceptable values for the operational phase of the forecasting tool. The shapes of the scatterplots (Figure 8c,d) for the wave features are expectedly more spread out than the ones for Los Angeles due to the larger number of model points used for comparisons (referring to locations of wave buoys; Figure 5).

The Pearson correlation  $R_p$  values are quite low for the  $T_p$ , yet this is well awaited in operational forecast modelling practice for coastal, nearshore, and port areas, according to many researchers [26,27,31]. The Pearson correlation values for comparisons of modelled-measured wave periods (mean  $T_m$  or  $T_{m02}$  or  $T_p$ ) typically fall close to or even lower than  $R_p = 0.5$  (ranging from 0.3 to roughly 0.7), indicating very low skill scores of classic 3rd generation operational models for predicted wave periods, while significantly higher agreement is usually achieved for the wave heights, as is the case with our OFP. Thus, to our knowledge, there are not any operational forecast systems (with data-assimilation systems and offshore forecasts excluded) that show good correlations between model/field wave periods in coastal areas near ports. Several researchers (e.g., Chawla et al. [25]) further discuss this discrepancy, while others usually avoid quantitative comparisons of modelled-measured spectral wave periods [20–23,28,30].

#### 4.1.2. Integrated Models A/B vs. OFP Modelling Data

Model B (WAVE-L) has been upgraded from its previous versions [78,86,87] and its performance has been previously evaluated, both fundamentally by experimental data in laboratory flume scales and practically by field data in the Thessaloniki port area [17,18,79]. The encouraging model results referred to wave penetration and diffraction through port entrances (breakwater gaps) and roundheads of semi-infinite jetties or refraction due to shoaling bed formations. New features include a quasi-irregular wave generator at the open boundaries and modulated wave reflection from realistic solid boundaries for practical applications [18,79]. Table 4 and Figure 9 present the validation of the latest version of the model against SAPO/SAMOA OFP results based again on scatterplots and the abovementioned statistical measures. The comparison of mean wave direction,  $\varphi_i$ , is also included in the model evaluation analysis.

**Table 4.** Validation of Accu-Waves (mod 1) against SAPO/SAMOA (mod 2) models based on statistical measures: Percent Errors, PE (%), for maxima and means, and standard deviations, RMSE (m or sec or °),  $R_p$ , WSS, and HRP-index for the timeseries of significant wave height  $H_s$  or  $H_{mo}$ , peak spectral period,  $T_p$ , and mean direction of wave propagation,  $\varphi_i$ . Port of implementation: Algeciras.

Port	A: Wave Parameter	PE (%) Max $A_{mod-obs}$	PE (%) Mean $A_{mod-obs}$	PE (%) $\sigma_{A,mod-obs}$	RMSE (m or sec or °)	RMSE/ $A_{obs,max}$	$R_p$	WSS	HRP-Index
Algeciras	$H_{mo}$	18.4%	27.1%	8.60%	0.13	7.44%	0.88	0.91	0.99
	$T_p$	12.7%	0.24%	30.6%	3.78	21.3%	0.15	0.42	0.97
	$\varphi_i$	5.05%	13.7%	39.8%	61	17.9%	0.47	0.64	0.95

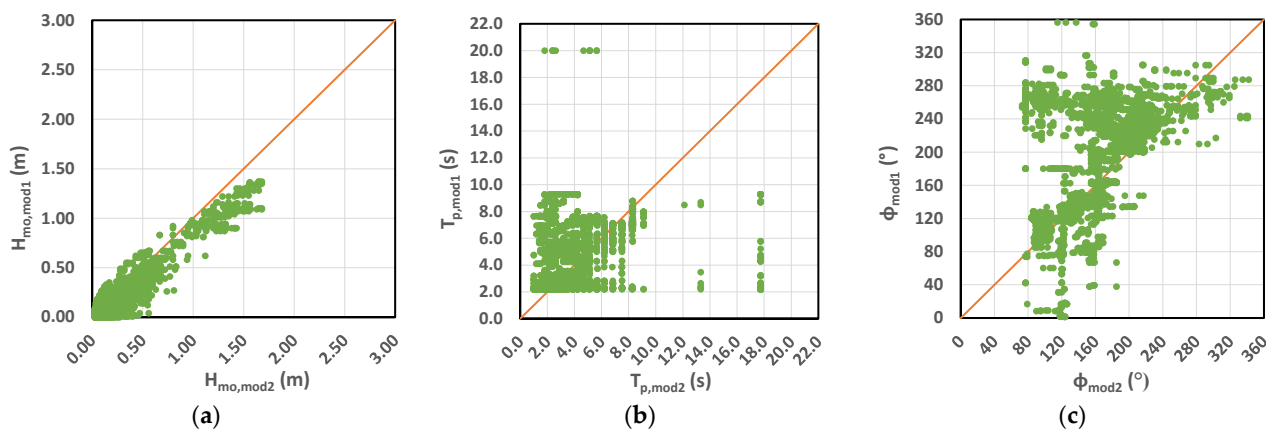


**Figure 9.** Correlation of Accu-Waves Models A+B results (mod 1) and SAPO/SAMOA OFP model output (mod 2) data by scatterplots of (a) significant wave height  $H_{mo}$ , (b) peak spectral period  $T_p$ , and (c) mean wave direction  $\varphi_i$  (right panel) values for the port of Algeciras.

The inter-model comparisons against the SAMOA WFS at the port of Algeciras (SAPO, Puertos del Estado), based on  $H_{mo}$ , also range from very good to exceptional; the skill score and correlation are quite high ( $R_p$  and WSS around 0.9 and HRP-index > 0.99; Table 4). The percentage errors are considered to be small, <20%, with an RMSE lower than 8% of the critical maximum magnitude of  $H_{mo}$ . An interesting feature refers to the percent errors of  $T_p$ , which are quite small (PE < 13% and <1% for maxima and average, respectively; Table 3) with an RMSE < 22% of maxima simulated  $T_p$ . The shapes of the scatterplots (Figure 9) are very reasonable for  $H_{mo}$ , yet there are several discrepancies for  $T_p$  and  $\varphi_i$ . In general, the Accu-Waves Model A/B ensemble (TOMAWAC+WAVE-L) performs in acceptable agreement with the corresponding model of SAPO/SAMOA OFP. Note that the meteorological data sources feeding the two schemes are also different (NOAA vs. ECMWF, respectively). The latter is crucial in order to achieve agreement among models' output. In Algeciras, the modelled period values score quite low ( $R_p$  and WSS < 0.5; Table 4) in skill and correlation indices, but it can be said that this is a 'special' area due to its proximity to the Gibraltar Strait and the Atlantic Ocean. These are two distinct aquatic bodies, and the model output should confound various wave components from them (e.g., Atlantic swells), making the accuracy of simulations particularly difficult. Met-ocean OFPs usually tend to highly differ against each other (or fail against in situ records) in the prediction of mean direction for spectral wave propagation, especially in coastal areas. A favorable output of our WFS is the acceptable agreement of the two models' values for the mean wave propagation direction,  $\varphi_i$ . The correlation coefficient and skill score range from marginal to acceptable ( $R_p \approx 0.5$ , WSS > 0.6, HRP-index > 0.95; Table 4), which means that Model A can meet the operational forecasting needs for the main propagation characteristics of the spectral wave fields.

#### 4.2. Operational System Results

##### 4.2.1. Accu-Waves WFS Output in Near-Real-Time Forecast Mode

The WFS testing involves the integration of all model components [17,18], execution command, and control codes that implement the system's functions towards complete product delivery, allowing for testing as an integrated OFP. Both the demo *beta* version (Figure 10) and the final WFS output versions (Figures 11–13) were tested to validate the Accu-Waves OFP ability to meet the user-identified requirements in terms of reliability and easy use. The main goal of these tests was to increase confidence in the WFS output, seamless sharing, and transferability of the OFP outputs to end-users. The aim of the WFS tool is to provide a user interface for reliable forecast representations of 3-day wave characteristics (incl. sea level and currents) in 3 h prediction intervals depicting the essential sea-states in

the selected port basins, near navigation channels, along typical vessel approach routes, and around ports at distances of the order of 25 nautical miles.

The *Leaflet* technology for georeferencing on Google Maps allows the end user to apply very detailed resolution displays of the order of a few tens of meters for both Models A and B domains. Examples of the back-up demo version of the web-GIS app for Model A forecasts (Figure 10) and final output version illustrations of the Accu-Waves WFS product for Model A (Figures 11 and 12) and Model B (Figure 13) refer to the 2-D horizontal fields of spectral wave characteristics ( $H_{m0}$  and  $\varphi_i$ ) in the wider areas of the ports of Antwerp (North Sea), Algeciras and Genova (Mediterranean Sea), Novorossiysk (Black Sea), Le Havre and Halifax (East and West Atlantic), Fujairah (Persian Gulf), Bangkok (Gulf of Siam, South China Sea), Thessaloniki and Piraeus (Aegean Sea). Figures 10–12 also pertain insert graphs of the timeseries of Sea Surface Elevation (m) due to the prevailing meteorological conditions (incl. storm surges or depressions) and tidal effects locally for a 3-day period (by Model H simulations). The features of barotropic currents (by Model H results) are also provided in the final Accu-Waves OFP output (Figures 11 and 12).

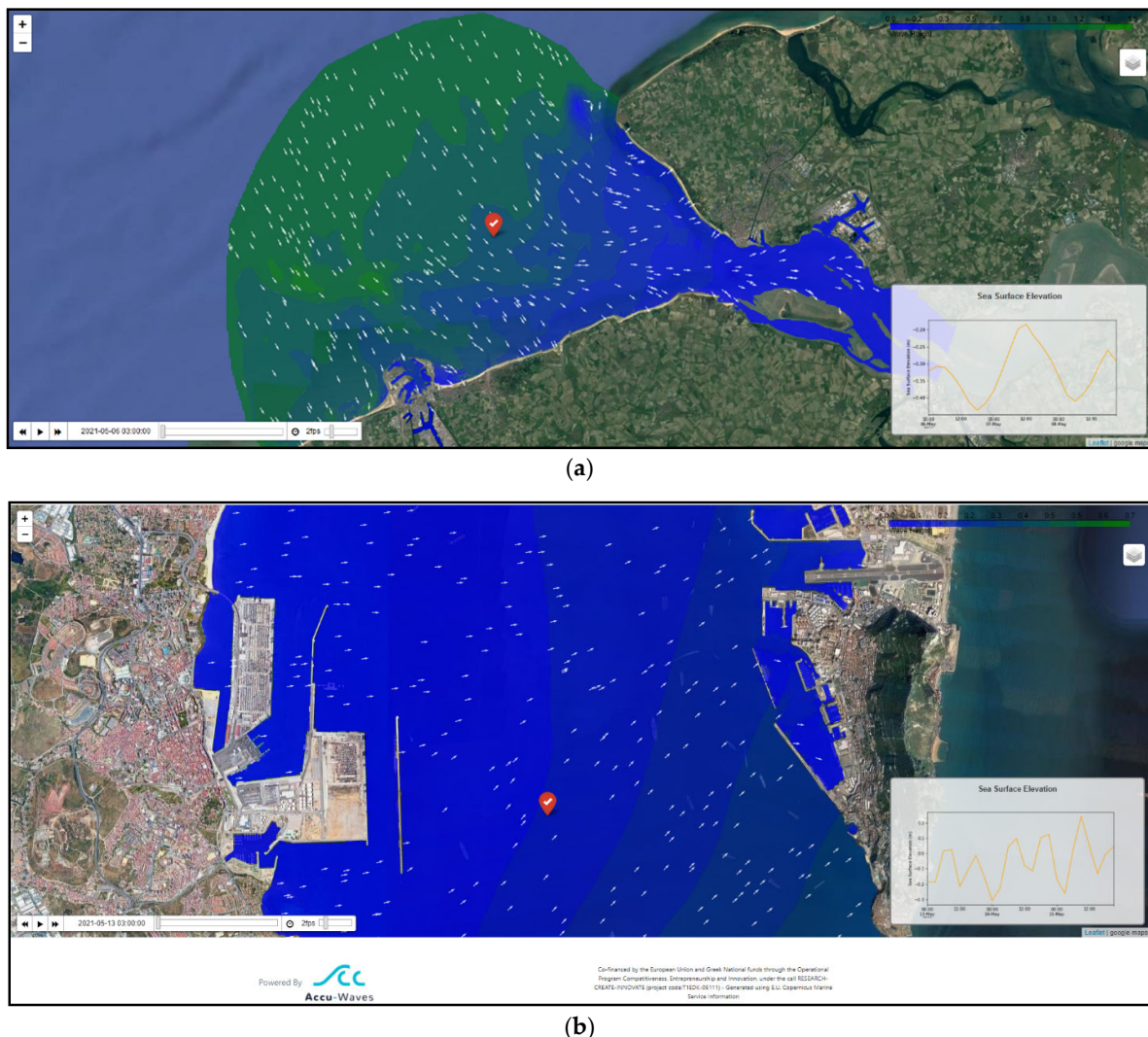
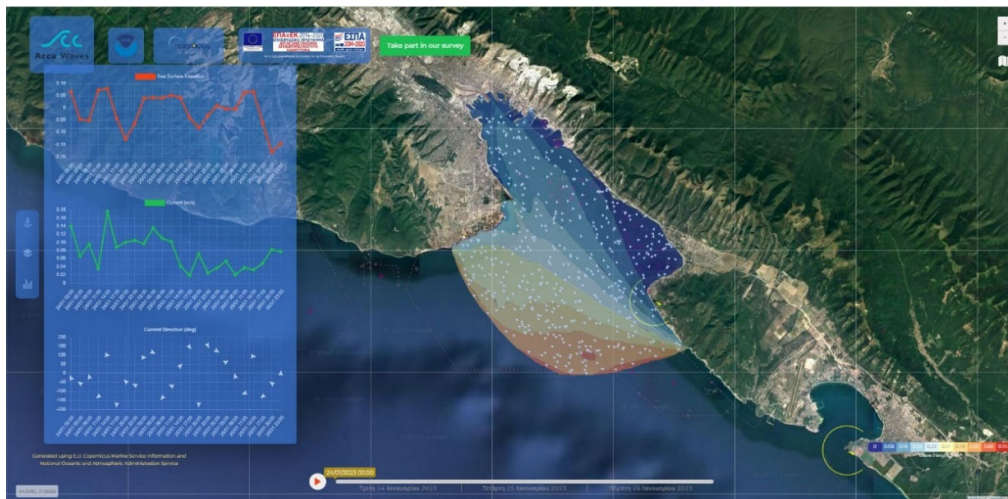
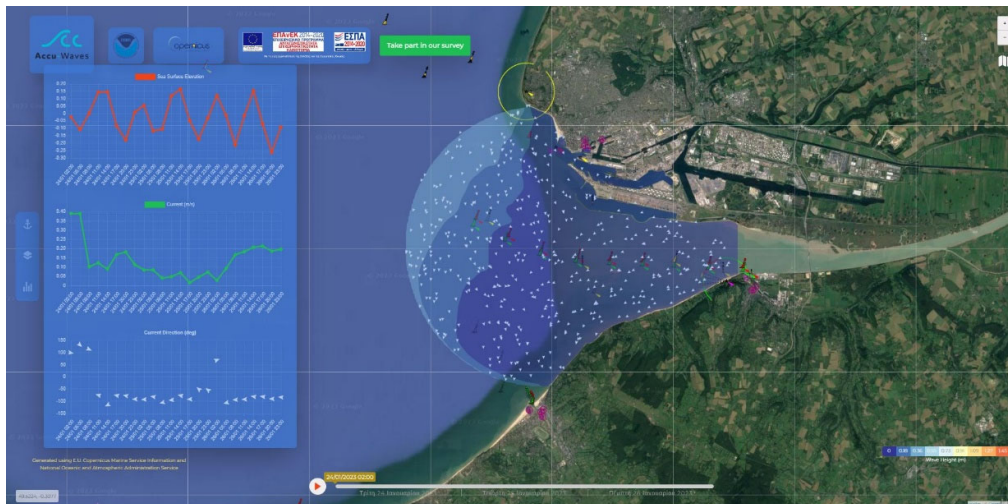


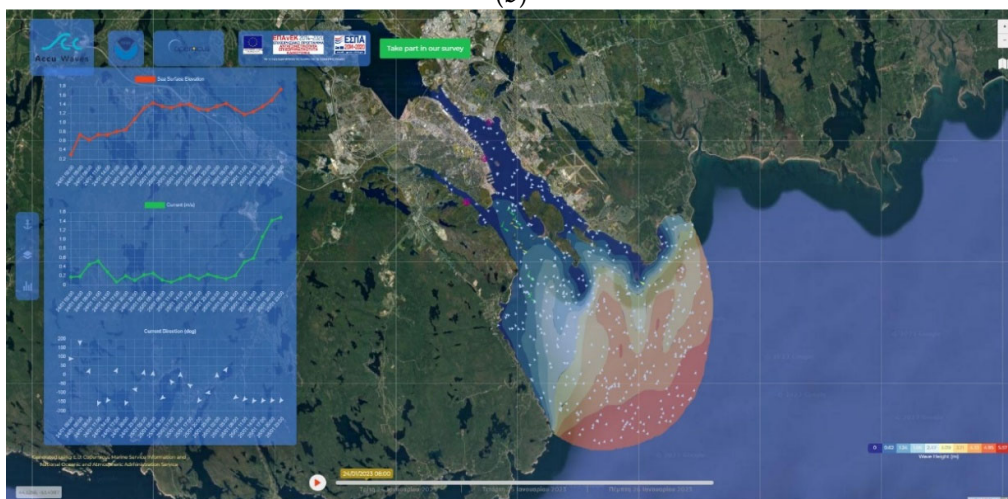
**Figure 10.** Demo version (back-up visual output) of the web-GIS app: illustration of Model A forecasts for 2-D horizontal fields of spectral wave characteristics ( $H_{m0}$  by colour contours;  $\varphi_i$  by vectors) in the wider areas of (a) Antwerp and (b) Algeciras ports (upper and lower graphs, respectively) on selected days of May 2021. Insert graphs: Sea Surface Elevation (m) 3-day time series.



(a)

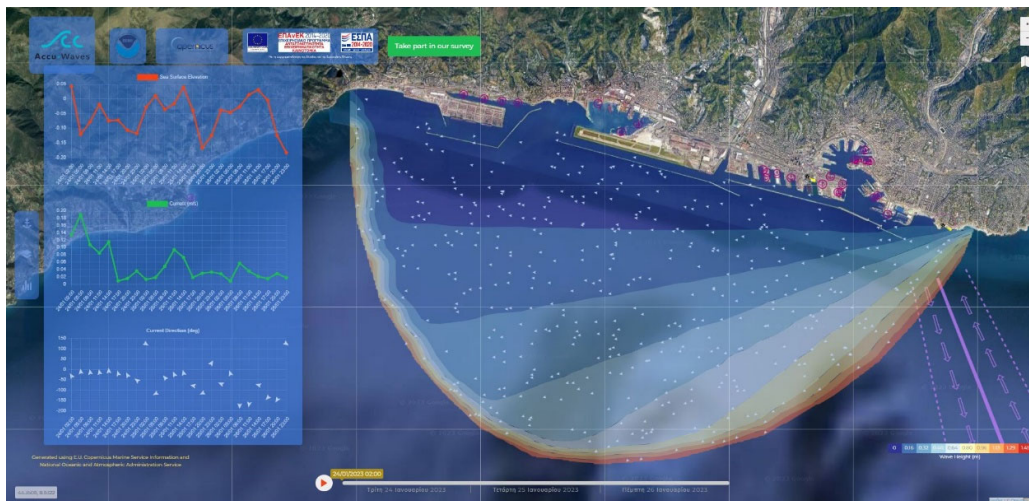


(b)

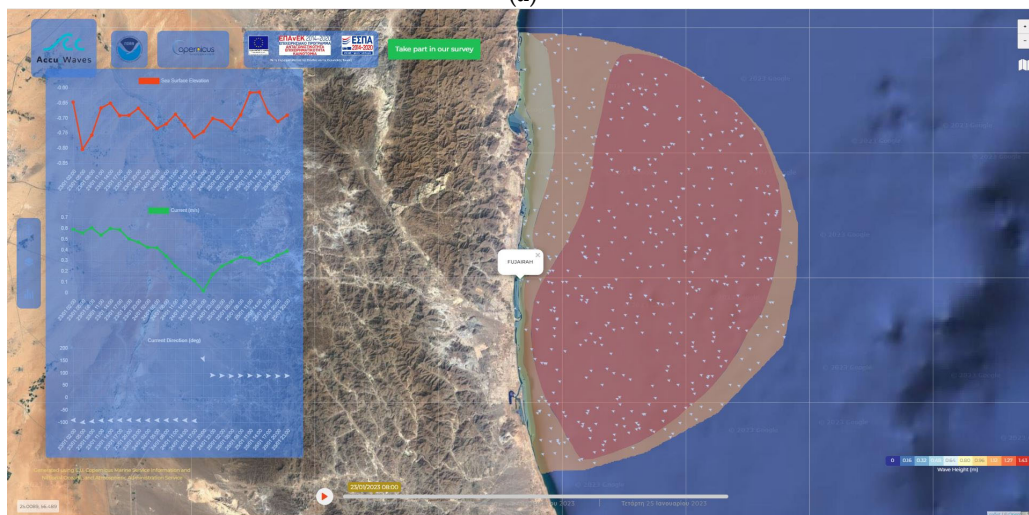


(c)

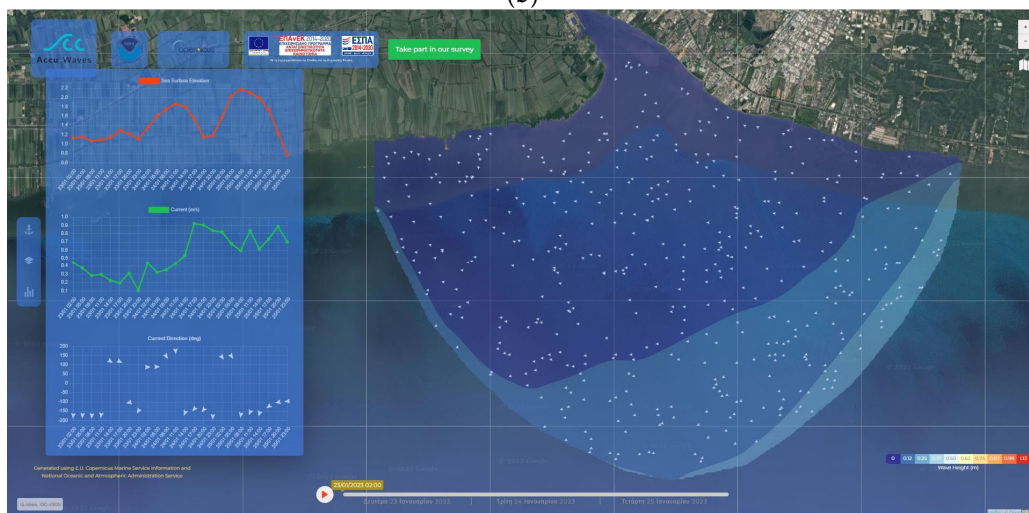
**Figure 11.** Final output version (provided freely) of the Accu-Waves WFS on the web-GIS app: illustration of Model A forecasts for 2-D horizontal fields of spectral wave characteristics ( $H_{m0}$  and  $\varphi_i$ ) in the wider areas of (a) Novorossiysk (Black Sea), (b) Le Havre, and (c) Halifax (East and West Atlantic) ports (**upper, mid, and lower graphs**, respectively) in January 2023. The insert timeseries graphs show the Sea Surface Elevation (m) due to the prevailing meteorological conditions and tidal effects locally for a 3-day period, the Barotropic Currents' velocity (m/s), and direction ( $^{\circ}$ ).



(a)



(b)



(c)

**Figure 12.** Final output version (provided freely) of the Accu-Waves WFS on the web-GIS app: illustration of Model A forecasts for 2-D horizontal fields of spectral wave characteristics ( $H_{m0}$  and  $\varphi_i$ ) in the wider areas of (a) Genova (Mediterranean), (b) Fujairah (Persian Gulf), and (c) Bangkok (Gulf of Siam, South China Sea) ports (**upper, mid, and lower graphs**, respectively) in January 2023. The insert timeseries graphs are similar to the ones in Figure 11.





**Figure 13.** Final output version (provided freely) of the Accu-Waves WFS on the web-GIS app: illustration of Model B forecasts for 2-D horizontal fields of characteristic wave height ( $H_s$ ) in the ports of (a) Thessaloniki, and (b) Piraeus (Aegean Sea, Mediterranean; **upper** and **lower** graphs, respectively) in January 2023.

By moving the cursor over the relevant wave direction vector arrows, the user can be informed about the detailed numerical values of all wave characteristics ( $H_{m0}$ ,  $T_p$ ,  $\varphi_i$ ) for mixed-seas environments, i.e., including both wind waves and swell, when the latter is present and adequately strong. A very fine resolution of the order of a few meters ( $dx = 2.5\text{--}3.5$  m) is ensured within Accu-Waves OFF thanks to Model B applied inside the port basins and the leeside of coastal and harbor structures (Figure 13).

The left-side menu of the web-GIS app (Figure 13 graphs) additionally provides the end-user with the ability to choose between Model A or B forecast depictions and the Model H output pop-up. Another GIS design option is the dynamic display of the color scale based on the 3-day forecast. With this option, the end-user has the ability to easily color-code the points with the highest wave height values, even in milder weather and calm sea conditions. Such a feature is beneficial for large ships approaching the port but

significantly more useful for the safety of smaller vessels and boats moving within the harbored areas.

#### 4.2.2. Models A/B Forecast Output under Scenarios of Moderate to Rough Sea Conditions

Following the verification of the OFP modelling component in the ports of Algeciras, Antwerp, and Los Angeles, adding to validation against experimental data and in situ observations at Thessaloniki harbor [17,18], we further provide typical results of our WFS model output empirically inspected over each port domain for both average and high sea conditions. Feedback from coastal/hydraulic/port engineering consultant experts was then considered (see Acknowledgements for details). Thus, several tests were set up to check on the models' performance under characteristic scenarios of moderate, rough, and very rough wave conditions (according to the Douglas Sea Scale) singular to every port and their adjacent marine bodies. The produced images (Figures 14 and 15, and all at Supplementary Materials S3 and S4) show the plan view maps of significant wave height (pseudo- $H_s$  for Model B or  $H_{m0}$  for Model A) and mean wave propagation direction ( $\varphi_i$ ) in vector form. The consistency of model response to the effects of detailed local bathymetric and topographic features was empirically evaluated by comparing, e.g., model runs with and without the inclusion of solid boundaries' proper configuration in every port to achieve a better representation of (partial) reflection from the waterfront.

In intermediate-depth and shallow waters, the evolution of the significant wave height and propagation direction was evaluated based, mainly, on the effects of depth-limited wave breaking and refraction. In regions near port structures and navigational formations, the existence of local morphological peculiarities of the seabed, e.g., shoals, reefs, steep bottom dips, dredging areas, entrance channels, etc., was also assessed in terms of transformations in wave characteristics. Near land and insular boundaries, the partial (or total) reflection of waves (Model B) due to sloping and vertical waterfronts of harbor works was also checked based on the interactions of wave components. Peculiarities of the simulated wave fields, such as the formation of standing waves (seaport seiches), square wave and cross-sea phenomena, wave diffraction-related patterns, etc., were also examined. This was performed on the basis of identifying the known weaknesses (diffraction and reflection at roundheads, port entrances, and engineered seafronts) and strengths of spectral phase-averaged Model A or phase-resolving Model B in terms of feasibly serving the practical needs of the OFP users and the objective of the Accu-Waves final output. In Model A domains, especially in areas with adequate fetch, the generation and propagation of secondary waves induced by local winds were also evaluated. Finally, in meso- and macro-tidal port areas, where strong sea level variations influence the local water levels, tests were performed for several MSL scenarios in the wave models.

**Table 5.** Scenarios for testing moderate to rough wave conditions with Model A simulations in the port of Barcelona (Spain, West Mediterranean Sea). The given parameters refer to the significant wave height,  $H_{m0}$ , peak spectral period,  $T_p$ , mean direction of wave propagation,  $\varphi_i$ , and wind speed zonal and meridional components  $W_x$  and  $W_y$ .

Scenarios	$H_{m0}$ (m)	$T_p$ (s)	$\varphi_i$ (°)	Sector	Wind Speed	
					$W_x$ (m/s)	$W_y$ (m/s)
A#1	1.80	4.5	30	S-SW	6.00	10.39
A#2	3.80	10	315	SE	−14.14	14.14
A#3	3.80	10	30	S-SW	10.00	17.32

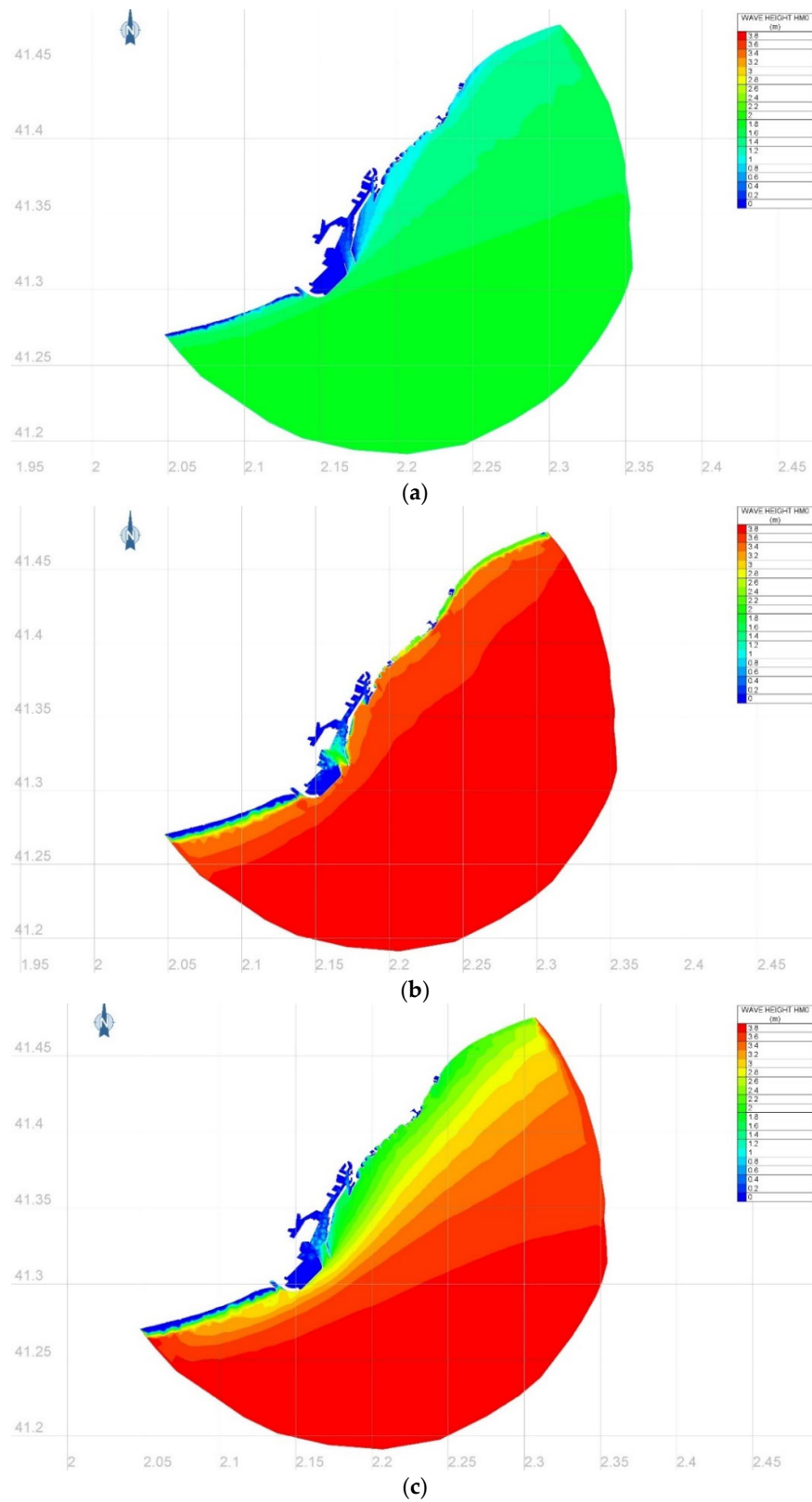


**Figure 14.** Characteristic results for  $H_{mo}$  (m) from the operational WFS component of Model A over the continental shelf around the port of Barcelona (Spain, West Mediterranean Sea) during S-SW and S-SE sector moderate to rough wave conditions for scenarios (a) A#1, (b) A#2, and (c) A#3 from Table 5.

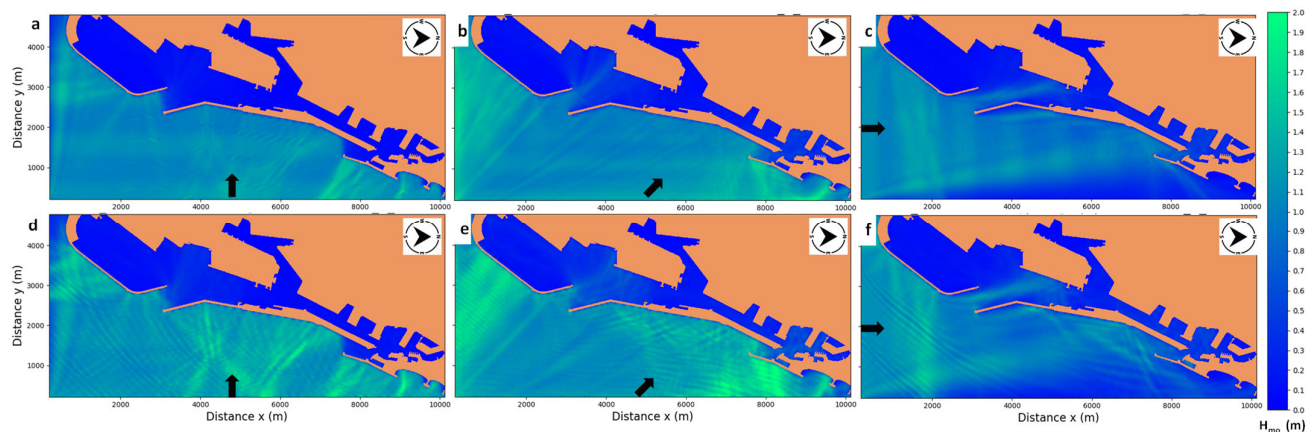


**Figure 15.** Characteristic results for  $H_s$  (m) from the operational WFS component of Model B on a harbor-basin scale in the port of Barcelona (Spain, West Mediterranean Sea) during E (a,d), SE (b,e), and S (c,f) sector incoming waves of  $H_s = 1$  m and  $T = 8$  s (a–c) or  $T = 12$  s (d–f); port map orientation turned  $90^\circ$  clockwise. Black arrows represent the main wind “flow-towards” vector.

The moderate-to-rough wave condition scenarios of the operational models were created in such a way to include inter-comparing variations of wave period/height/direction, wind speed, and sea level/currents. For example, if two scenarios referred to the same  $\varphi_i$  but included different  $H_{m0}$  and/or  $T_p$ , we evaluated the consistency of the respective model results in realistically reproducing the relation between different input and output wave characteristics among the test cases. In terms of Model A and B interaction, the incident wave field in the nested model areas and the wave generator boundaries were also checked for consistency in wave propagation characteristics, i.e., rationality of wave direction angles, formation of wave caustics, emergence of non-physical wave interference, etc. The lateral boundary conditions were also checked, while wave interaction with nearby solid boundaries that may create unnatural reflections and standing waves or unreasonable wave energy damping was further assessed. The homogeneity and consistency of the generated waves at the open boundaries were evaluated, too. For Model B, the perpendicular open boundaries in the peripheral zone of the simulation domain and the performance of the sponge layers were also rated.

The main example presented here is the port of Barcelona (results of evaluative tests for all the rest of the ports are presented in Supplementary Materials S3 and S4 for Models A and B, respectively). Tables 5 and 6 present the scenarios concerning moderate to rough sea states ( $1.5 < H_{m0} < 4$  m) and typical ( $H_s = 1$  m; scales easy due to the nature of the HMS phase-resolving model) wave conditions in the area around and inside the port of Barcelona (Spain, West Mediterranean Sea), for Models A and B, respectively. Note that for the operational forecasts, Model B initiates runs with whatever wave height/period/direction values Model A feeds to them. Only for the above scenario runs, we assigned unity scale wave height ( $H_s = 1$  m) on the wave generator line of Model B strictly for depictional reasons, i.e., in order to easily trace the amount of decrease (due to breaking, shoaling, etc.) and increase (in case of reflection from waterfronts and port structures) caused to the wave height values.

The parametric analysis refers to  $H_{m0}$ ,  $T_p$ ,  $\varphi_i$ , zonal N-S and meridional W-E components of wind speed,  $W_x$  and  $W_y$ , and the typical time of simulation (duration of the wave storm),  $t_{sim}$ . Wind speeds blowing from west to east and south to north are considered positive. The Sea Level Elevation (SLE, m) is further provided for several ports in meso- and macro-tidal coastal environments, i.e., with significant effects of astronomical tides on the MSL for the various wave scenarios. It is noted that the angle of wave propagation direction is expressed relatively to north, with a positive clockwise rotation. For example, an  $\varphi_i = 0^\circ$  corresponds to waves propagating from south to north, i.e., the arrow denotes a “flow-towards” vector. Thus, an angle of  $\varphi_i = 90^\circ$  stands for waves coming from the west

and moving towards the east, while  $\varphi_i = 315^\circ$  indicates waves coming from the south-east and moving towards the north-west.

**Table 6.** Relevant scenarios for Model B tests of wave agitation in the port of Barcelona (Spain). Given parameters refer to the significant wave height,  $H_s$ , a characteristic period,  $T$ , the mean direction of wave propagation,  $\varphi_i$ , and the typical time of simulation (e.g., the duration of a wave storm),  $t_{sim}$ .

Scenarios	$H_s$ (m)	$T$ (s)	$\varphi_i$ ( $^\circ$ )	Sector	$t_{sim}$ (s)
B#1 (2.1)	1.00	8.00	270	E	2100
B#2 (2.2)	1.00	8.00	315	SE	2100
B#3 (2.3)	1.00	8.00	0	S	2100
B#4 (3.1)	1.00	12.0	270	E	2100
B#5 (3.2)	1.00	12.0	315	SE	2100
B#6 (3.3)	1.00	12.0	0	S	2100

The results for moderate-to-rough and normal wave conditions with Model A and B tests in the port of Barcelona are provided in Figures 14 and 15, respectively. Figure 16 illustrates the Model A and B domains' bathymetries for comparative reasons. Figure 14 presents Model A results about cases of S-SW and S-SE sector moderate to rough wave conditions of  $H_{m0} = 1.8\text{--}3.8$  m, with  $T_p = 4.5\text{--}10$  s, and winds blowing with speed up to 20 m/s (9 Bf; strong/severe gale) from the North African cyclogenesis centers towards the Iberian Peninsula for scenarios A#1-3 of Table 5. Figure 16b presents the bathymetry of Model A domain in Barcelona port. The modelled wave fields in the port approach area show a wave focusing before the port basin entrance. Wave penetration in the central port is considered normal, while penetration through the secondary (northern) inlet and along the northbound wharves outside the main port may not be very accurately captured, considering the inability of Model A to simulate wave diffraction and reflection. This is not judged as a serious disadvantage of the OFP since Model B covers the demand for more astute predictions on the leeward side of port structures and primary jetties, where wave heights can be underestimated by spectral models (see following comments).

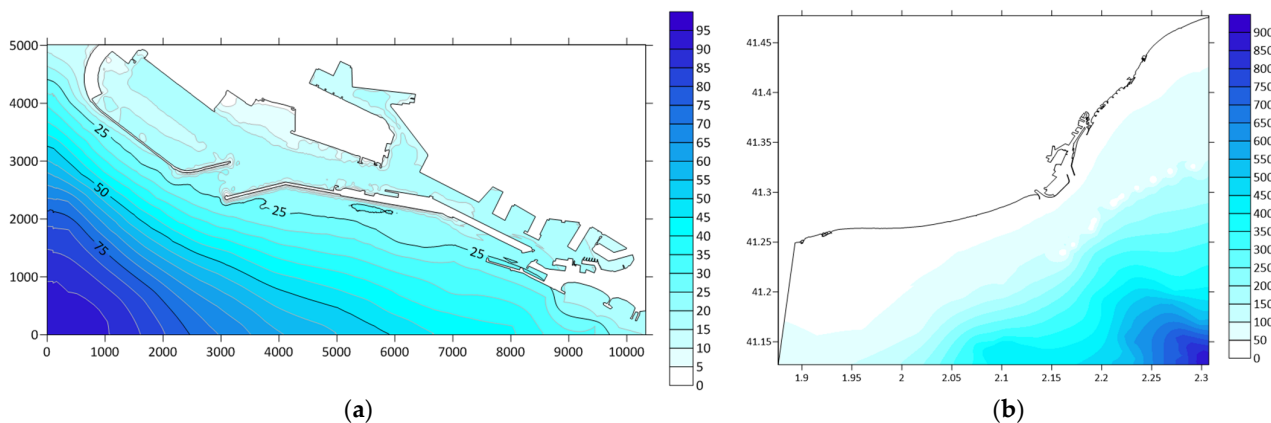


**Figure 16.** Barcelona port bathymetry: colour bars correspond to seabed level below Still Water Level (d, in m) derived from measurements and bathymetric surveys incorporated in local nautical maps (from National Hydrographic Survey Agencies) and the latest Navionics products. (a) Bathymetry map of Model B domain turned  $90^\circ$  clockwise in a virtual orthonormal coordinate system in meters; start of x- and y-axis (0,0) on low left corner. (b) Bathymetry map of Model A domain in a WGS84-projection polar coordinate system in decimal degrees ( $^\circ$ ).

The reduction in wave heights in nearshore shallow areas around the port is obvious, and the general patterns of the wave propagation direction due to refraction are presented reliably, following the underlying seabed contours. For Scenario A#3, waves inside the southern port basin are observed, but their height and extent seem limited for a 9 Bf wind

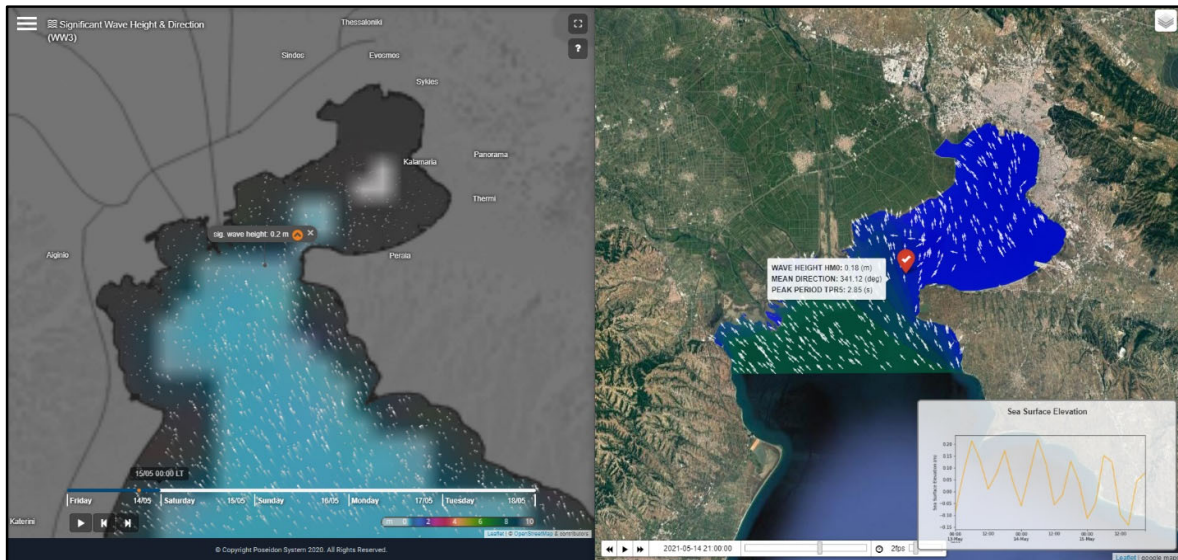
with a reckoned fetch of many kilometers. In general, based on the results of Supplementary Materials S3 in all 50 ports, the modelled wave fields at the harbor entrances and near the breakwaters reveal the expected wave focusing and blocking, respectively. The depictions of Model A results in all ports (Supplementary Materials S3 applications) clearly portray the wave penetration in the port basins with a directional spreading of spectral wave propagation, especially along dredged bed channels in port approaches.

Figure 15 presents model B results about cases of E (a, d), SE (b, e), and S (c, f) sector incoming waves of  $H_s = 1$  m for wind-induced seas  $T = 8$  s (a, b, c) and swell  $T = 12$  s (d, e, f). Figure 16a presents the bathymetry of the Model B domain in Barcelona port. In general, the wave penetration at the main port is low. Stronger reflections are observed in the areas of the windward piers with vertical fronts north and south of the port. Wave attenuation by the harbor's breakwaters is evident. The OFP can achieve a very detailed depiction of the wave height evolution on the leeward side of the jetties and protective structures near the port entrance when there is an incident wave attack from the S and SE sectors (Figure 15c,e,f). Moreover, there is also wave agitation in the secondary north harbor for the SE swell case (Figure 15e), evident even on berth positions and protected internal waterfronts (crucial for port managers and berth positioning). Wave reflection in the windward jetty areas with vertical fronts north and south of the harbor is stronger. In general, the reflections on the external port area are much higher than those inside the port basin, except from the main port-center quay wall during SE wind-waves (Figure 15c). The wave penetration at the main entrance of the port is considered normal due to the direction of the incoming waves. The observed increase in wave energy due to reflection of E and SE incoming waves at the north of the port and near the area of the coastal protection project is judged to be quite large and probably related to the short distance from the boundary condition of the computational domain (right parts of Figure 15b,d,e graphs). The wave penetration at the main entrance of the port is significant and considered normal due to the direction of the incident waves. The depictions of Model B results in all ports (see portfolio in Supplementary Materials S4) show pronounced wave diffraction patterns everywhere, with a rational representation of wave attenuation inside the port basins. In most of the applications depicted in Supplementary Materials S4, the wave penetration in the port basins is clearly portrayed, as are the directionality and refraction of waves, especially along the dredged bed channels of the port approaches and entrances. The wave reflection outside the port on the windward jetty, pier, and breakwater fronts may seem exaggerated in some cases, but we did not trace a strong influence of reflected waves in the designated offshore anchorages, which is crucial for port managers and seafarers. In exceptional cases of wave propagation parallel to or along the breakwaters (Supplementary Materials S4), Model B did not exaggerate in the prediction of wave energy dissipation and diffraction about the roundheads.

#### 4.3. Tests of Accu-Waves OFP Verification against other Forecasts and Field Data

The extended literature review (Section 2) has shown that most of the open marine forecast tools cover wider areas of the coastal zone, the open sea, and oceans and therefore are not ideally intended to support, via detailed wave forecasts, decisions for ships approaching and navigating in port areas. However, in view of the need to build such a Decision Support System (DSS), we consider it appropriate to compare the predictions of Accu-Waves OFP with other similar applications, which every ship navigator and captain or port management authority usually consults. This is especially needed for the difficult task of validating the predictive ability of our WFS in terms of waves' directionality. As an example, we compare the accuracy of our OFP, tool with the output of the established Mediterranean Sea's Poseidon system [113] for the area of Thessaloniki port (Thermaikos Gulf; Figure 17). The visual comparison is favorable for the Accu-Waves OFP portraying a rational accordancy of the predicted mean wave direction component over the continental shelf area with the relevant Poseidon product (WaveWatch-II forecasts). An obvious advantage of the Accu-Waves OFP is the higher resolution and the focus on nearshore

scales for port-proximal navigation. The aforementioned inference is corroborated by a comparison of our OFP output with the ABPA [114] product of the Puertos del Estado WFS infrastructure at the port of Algeciras (Figure 18). The portrayal of wind-wave propagation by the two OFPs is almost identical, achieving refined accuracy in the port approach area of the Gulf of Algeciras.



**Figure 17.** Comparison of areal coverage and maximum achieved resolution results of WFS modelled  $H_{m0}$  (m) and  $\varphi_i$  (by vector arrows) with WaveWatch-III from the Poseidon system (left graph) and with TOMAWAC (Model A) from the Accu-Waves OFP (right graph) for the area of Thessaloniki, Greece (North Aegean Sea, Mediterranean; 14 May 2021; 21:00UTM). The Accu-Waves system is complementary to systems such as Poseidon in terms of dynamical downscaling and focusing on nearshore areas, coastal zones, and ports.

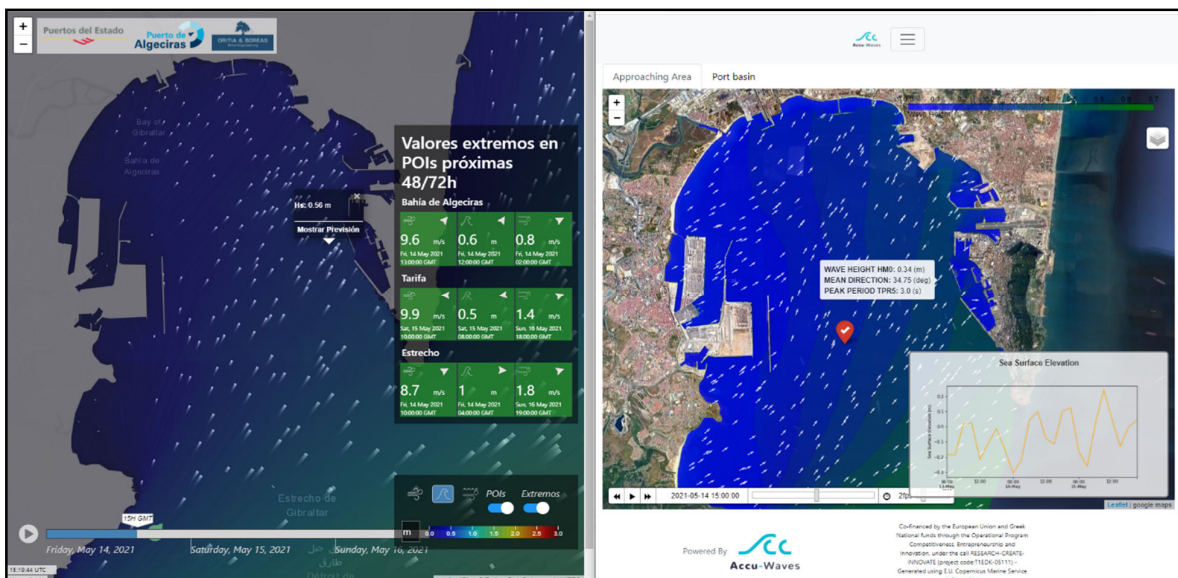


**Figure 18.** Comparative visualization of WFS model results between SAPO/SAMOA (left graph) and Accu-Waves (right graph) products of simulated  $H_{m0}$  (m) and  $\varphi_i$  (by vector arrows) in the broader Algeciras port area (on 15 May 2021, at 3:00). Accu-Waves OFP compares well with the established local forecast system of Puertos del Estado.

Furthermore, the performance of the Accu-Waves model ensemble WFS is cross-checked for an extreme case of a quite impressive wave event recorded by the Puertos del Estado's buoy of Punta Carnero (Lon: 5.42° W, Lat: 36.07° N, Data Sampling: 60 Min, Mooring Depth: 40 m, 1st record: 11 November 2010, Type of sensor: Directional, Model: WatchKeeper), stationed in the coastal waters along the entrance of the Bay of Gibraltar, where the Port of Algeciras is located. Figure 19 (upper graph) shows the raw data (provided courtesy of Puertos del Estado field recordings) of timeseries evolution for significant  $H_{m0}$  and maximum  $H_{max}$  wave heights from 2 April 2022 to 5 April 2022 covering a severe wave storm. The rough sea conditions started off with a  $H_{m0} = 2$  m and an  $H_{max} = 3.6$  m during the afternoon of 3 April 2022, and in two days, they reached a very high seas status of short-term values around  $H_{m0} \geq 6$  m with a recorded extreme of  $H_{max} = 10.94$  m during the night of 5 April 2022. The latter situation typically occurs for a very short time span, e.g., tens of minutes up to a few hours; the in situ recorded signal shows recurring high peaks in the wave height offshore Algeciras for less than 8 h. For typical ocean OFPs, it is admittedly hard to exactly reproduce such an extreme wave incident, as WFS models run and produce results in an averaged condition mode (e.g., hourly or 3-hourly, etc.). Therefore, some peaks in the continuously recorded wave state, which may be exceptionally high, usually fail to be simulated. However, Accu-Waves output achieves good accuracy (shown by the following post-processing of model results).

Accordingly, the Accu-Waves WFS output achieves predictions of high significant wave heights of  $H_{m0} > 5.54$  m, locally reaching values of  $H_{m0} = 5.92$  m near the coast of Punta Carnero (Figure 19; lower map). The corresponding modelled peak spectral periods range between  $T_p = 9.83$ – $11.18$  s for each 3-hourly sea state simulation. Based on Goda's spectral wave theory [115], we can calculate the characteristic ranging values of the Maximum Wave Height,  $H_{max}$ , for irregular waves according to the formula:  $H_{max} = k \times H_{m0}$ , where  $k$  ranges between 1.515 and 1.856 for 100–1000 recorded individual waves, respectively, in an irregular wave train. For a 3 h simulated time interval,  $t_{sim}$ , the rough estimate of the number of individual energetic wave components,  $n$ , would be ranging between  $n = t_{sim}/T_p = 10,800/(9.83\text{--}11.18) = 1099\text{--}966$  wave records. Thus, if our corresponding WFS results fluctuate between  $H_{m0} = 5.54$ – $5.92$  m, then the OFP's predicted wave height maxima correspond to values between  $H_{max} = 10.21$ – $10.49$  m and  $H_{max} = 10.91$ – $11.21$  m, depending on the relevant  $T_p$ . These values are very close to the in situ recorded  $H_{max} = 10.94$  m values by the wave buoy. The bias percentages score between the ranges of  $PE = -6.66\%$ – $-4.11\%$  and  $PE = -0.26$ – $2.46\%$ , which are practically very low values ( $0.2\% < |PE| < 6.7\%$ ), denoting a high-performance skill of Model A for the case of abnormally large waves. The achieved PE of modelled  $H_{m0}$  (and consequently calculated  $H_{max}$ ) values, based on the observed ones by the buoy, is practically miniscule. A ship captain and a port traffic manager need to know if a storm wave height will increase enough over a rough extreme threshold, i.e., knowing in advance that  $H_{max}$  will exceed 10 m would be sufficient information for them to take precautionary measures. In conclusion, the WFS model predictions can be considered reliable, even for extreme cases of storm waves, and the Accu-Waves OFP is regarded as producing efficient estimations of severe sea states within a coastal natural hazard prediction framework.



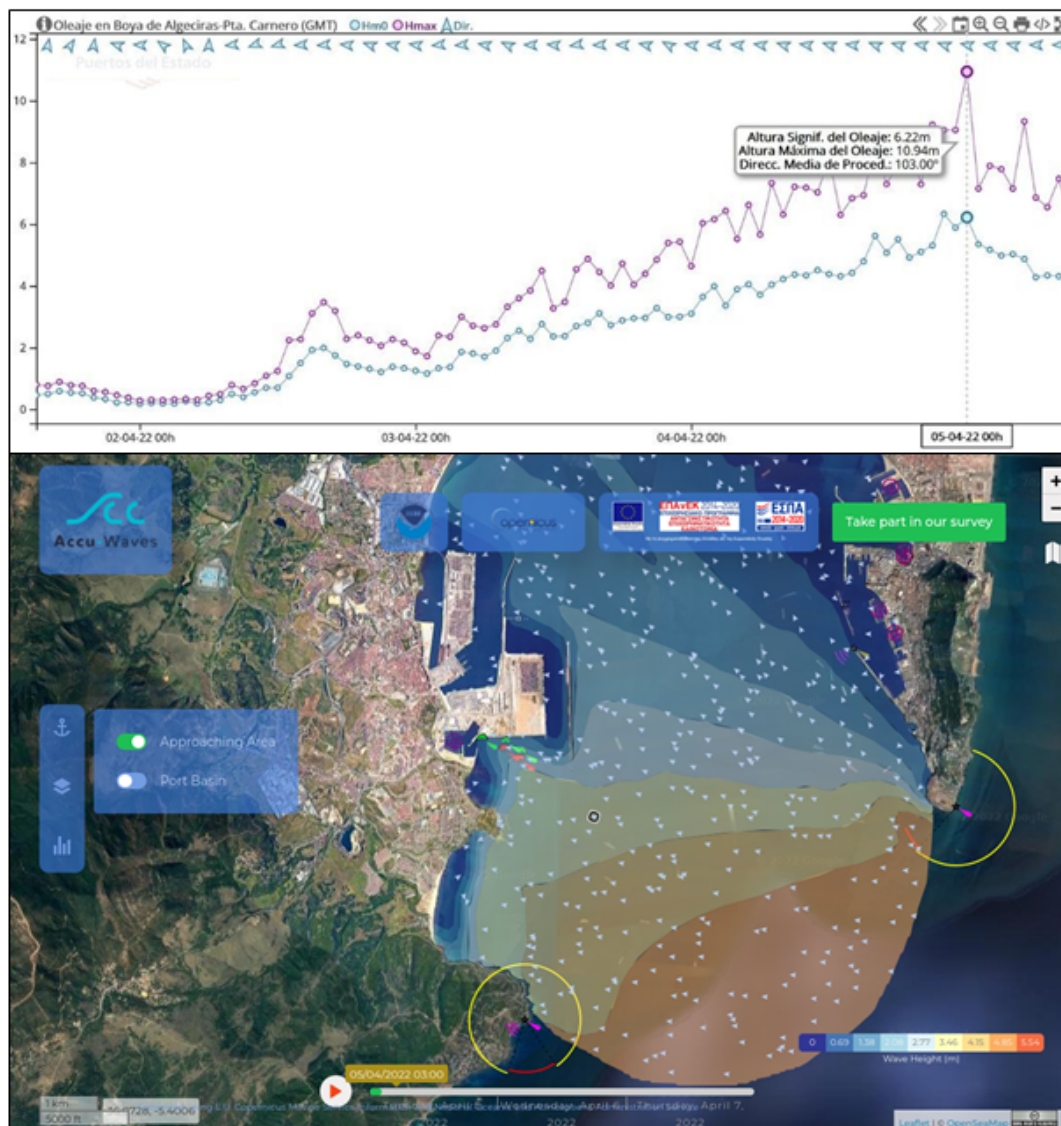


**Figure 19.** Comparison of Accu-Waves WFS model results (**lower map**) against in situ observations of wave height (**upper graph**; provided by courtesy of Puertos del Estado infrastructure) from the wave buoy at Punta Carnero (marked with a yellow circle and a purple mark in the low center of the **lower map**). Upper graph:  $H_{mo}$  (m) and  $H_{max}$  (m) with green/blue and purple dotted lines, respectively, recorded by the Punta Carnero coastal wave buoy; time series from 2 April 2022 to 5 April 2022 covering the entire storm wave event. Lower map: typical Accu-Waves WFS product depicting a 2-D map of predicted  $H_{mo}$  (m) in the broader area of Algeciras port (on 5 April 2022, at 3:00).

### 5. Discussion

A wide range of performance tests were designed and applied to ensure that the OFP and the hardware infrastructure can handle the intended computational load for model execution and interaction during a daily cycle, during which needed resources are steadily increased until a consummation plateau is reached, or the system fails. The task execution mechanism (Figure 20), as well as its scalability, is a key comparative advantage of the current OFP implementation. Accu-Waves, beyond a state-of-the-art attempt at the academic realm, is a novel technical product combining multiple simulation models with a very challenging operational undertaking. Its unique international character is signified by the involvement of 50 important ports spread out around the globe. The bold aspect of the OFP is demonstrated by the arduous work, which including a very large number of different elements that are required to be up-to-date and available at specific times in

a daily schedule, serving data in a specific format in combination with many detailed parameterizations per port and marine region, and engaging several computational tools in the context of WFS realization. Leveraging open-data sources for basic input provides the Accu-Waves OFP with certain constraints, but with versatility too, as more implementations can be easily added in the future by minor modifications and dataset additions.

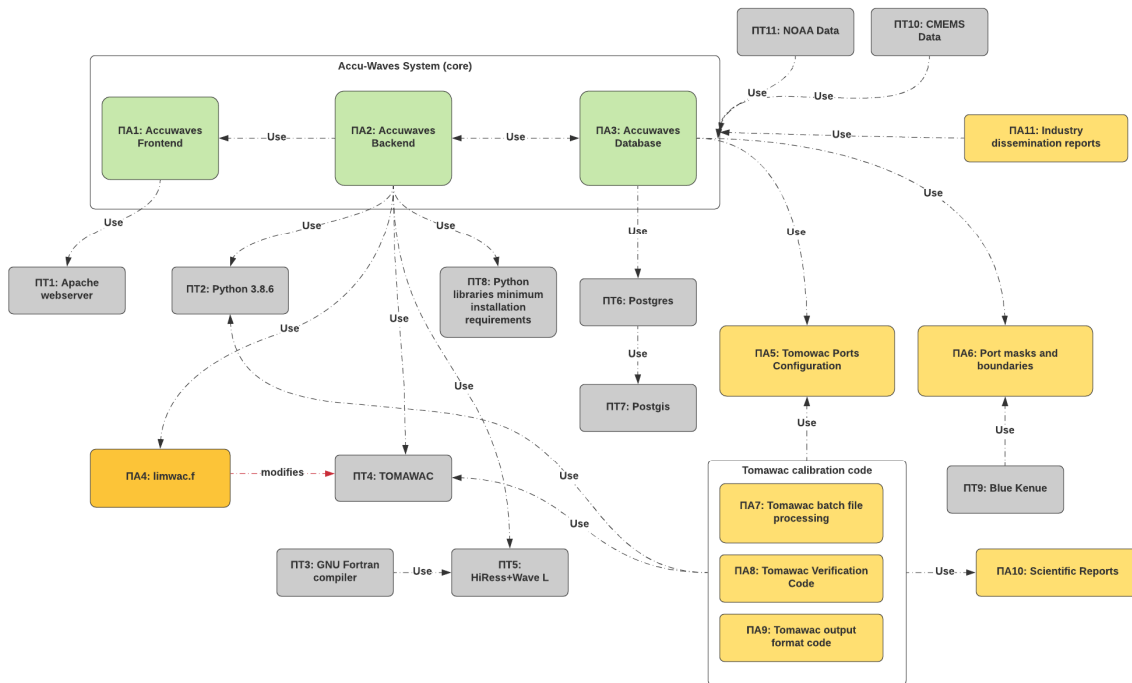


**Figure 20.** Summary of the sequencing components of Accu-Waves OFP delineating the interaction among produced model results and prior existing (external/patrimonial) info datasets (within the flowchart elements ΠA: Produced Results and ΠT: Preexisting Technology).

The computing system used for the current project is an HPE Proliant 380 server with an Intel Xeon 6138 processor with 40 logical cores and 128 GB of RAM. Practical model execution capabilities of the system ordain the initial implementation of Models H and A after the incipient system preparation (including retrieval of input data, file preparation and initial data management, translation, and storage filesystem setup). These results can back up an adequately full WFS product delivery in case of system failure. The Model B implementations in all selected ports within one day are a particularly hard task, requiring total execution times close to a one-day cycle with a fully working system capacity. This can dramatically reduce the hardware infrastructure’s lifetime and further increase the needs for service. Moreover, the additional storage space required for the generated files on a daily basis may reach up to 0.25 TB.

Frequent updates of topographic, bathymetric, and port configuration data, referring to probable technical construction interventions or dredging works, are also imperative in order to provide realistic depictions of the WFS product. The robustness of the model output by semi-automated validations against reliable field data, wherever available, is further set as a future goal to be pursued. Note that the forecast output for prevailing 3-houly sea-states in and around port basins is regularly updated every day in order to reduce the inherent fallacies in long-term wave data predictions; the forecasts’ quality degrades over time (3rd forecast day is more unreliable than the 1st day due to inaccuracy of meteorological forcing input). For the case of the Thessaloniki port validation of modelled output against field data [17,18] during the winter of 2019, the derived  $R_p$  values for the 1st to 2nd and 3rd simulated days degraded from 0.76 to 0.24 and 0.14, respectively. However, this finding may be circumstantial, conditionally subject to the triviality of the input data

in our analysis that depends on the restrictive nature of recorded/modelled local wave conditions.

Especially Model A is very susceptible to the quality, resolution, and reliability of atmospheric input data from NOAA's GFS and the boundary conditions of spectral wave characteristics provided by the relevant Copernicus Marine Forecast Systems around the globe. However, in general, when it comes to ship agitation in relatively confined spaces like ports or harbors, higher wave heights tend to have a more immediate and noticeable impact than wave periods (or frequencies of sea-surface oscillations) because they directly affect the ship's stability and maneuverability in shallow waters. Therefore, the main parameter that bothers ship masters/captains is the wave height, for which our models perform quite well. The problematic correlation values of compared model/field data for peak spectral periods are well awaited in the operational forecast modelling practice, especially for nearshore areas and ports, according to several researchers [26,27,31]. Researchers have reported  $R_p$  correlation values (for mean spectral periods  $T_m$  or  $T_{m02}$  and peak periods  $T_p$ ) that fall close to or even lower than  $R_p = 0.5$  (ranging from 0.3 to roughly 0.7), indicating very low skill scores of classic 3rd generation operational forecast models in terms of predicted wave periods, while significantly higher agreement is usually achieved for the wave heights, as is the case with our OFP. This issue (excluding data-assimilation systems and offshore forecasts) is discussed or implied by several publications [20–23,25,28,30]. Quite recently, Ricondo et al. [116] practically corroborate our conclusions, by presenting the same patterns of  $H_s$  and  $T_p$  scatter plots and respective values of correlation and error parameters. Overall, a more systematic investigation should take place, but this is out of the paper's scope and a potential subject of future studies.

The ability of the OFP to deliver very high-resolution outputs depend on the frequent service and the financial support of such a project, whose broader impact can be beneficial to a variety of players in the marine industry as well as the general public. The interaction of all the output produced by the Accu-Waves OFP is depicted in Figure 20 with yellow (intermediate results and parameterization) and green (central execution system) colors. The Technological Readiness Level (TRL) of the derived results is 6. Accordingly, the set of pre-existing available technologies (methods and tools) used during project implementation is portrayed in gray in Figure 20.

## 6. Summary and Conclusions

An aspiring, high-resolution OFP for waves and sea state prediction inside and around 50 very important ports worldwide is presented in this paper. Accu-Waves is an R&D prototype WFS product in the form of a web-GIS tool backed up by an integrated modelling suite for coupled wave simulations fed by modelled barotropic sea-level and current data. It can serve the needs for prediction of environmental factors useful to global navigation and the shipping industry. The produced OFP can support local or regional DSSs for port navigation management and shipping operations in coastal areas. An end-to-end integrated software suite of two high-resolution coastal models for spectral waves is therefore extensively validated against in situ observations from wave buoys and other similar, established forecast modelling applications. The Accu-Waves system incorporates a variety of diverse complex numerical data and processing codes within an automated, upscaled, parallel framework. Information is disseminated via a web-GIS app providing an easy-to-use interface for monitoring coastal- and port-scale met-ocean forecast data.

Validation of both the standalone and integrated models' performance proves that the WFS delivers quite reliable wave height predictions but presents discrepancies in terms of mean wave direction and peak periods. In general, the model skill metrics dictate that there is no imperative need for bias correction of the model outputs. Typically, the Accu-Waves' produced wave height data may be safely utilized for marine management purposes, yet the wave period data should be handled with much greater care since the large spread in the compared model vs. field observation values may limit the applicability of the OFP results. A continuous update and upgrade of the model verification system

within the Accu-Waves OFP should be further pursued to cover the entire globe. The high-resolution phase-averaged wave simulator (Model A) supported by the hydrodynamic solver for storm surges (Model H) proved to be a robust approach for reliable wind-wave and swell predictions. The OFP is completed by a very fine-scale phase-resolving wave model application, which seems very promising for redefining the WFS paradigm for ports. The only problem is the viability of model-suite execution, as Model B, when run in full-scale, burdens the computational system by occupying most of the resources.

Issues of the OFP's architecture are discussed in detail, including big-data management needs and difficulties of implementation. The job orchestration framework is programmed with the use of modern open-source applications fit-for-purpose within a product sustainability approach. Back-up procedures and contingency plans for database communication and model performance are also discussed, leading to the internationally designated software choice for the web-GIS results' dissemination.

The system has the ability to forecast sea conditions every three hours for three consecutive days in the short future at 50 globally important ports. The OFP provides the ability to display rather reliable predictions about the mean direction of surface currents, the sea level elevation, and the main wave characteristics in and around ports. Mixed swell/wind-wave seas can be simulated, and seiche effects from standing waves inside port basins can also be derived for safety purposes. The OFP presents in a reliable, easy-to-use, and coherent manner the information required by the end-user (vessel captains, ship owners, port managers, coastguard first-level responders, etc.) for timely decision-making related to navigation during vessels' calls to ports.

By comparison with other established WFSs and OFPs, Accu-Waves seems able to provide equally accurate forecasts yet with a highly increased spatial resolution, as proved by the validation against available field data (in situ observations of wave buoys) in the tested ports. The performance of our WFS in the case of extreme wave conditions, e.g., the higher than 10 m wave in Gibraltar Bay near Algeciras port during April 2022, is considered to be very satisfying, given the gravity of such events for safe shipping and the major risk of navigational accidents during exceptionally severe weather conditions. Of course, during stormy conditions, ship maneuvering is mainly influenced by dominating winds that push vessels against easy entrance. Yet, this kind of meteorological forecast product has already been provided to port-related stakeholders by several sources.

## 7. Outlook and Future Perspective

To operate the WFS to its full extent, i.e., running Models A and B for all port configurations, still remains a particularly arduous task due to the exaggeratedly increased computing power that is required, which can put any mini-scale forecast infrastructure system at operational risk. However, we have taken steps towards expansion possibilities in the design and implementation of the Accu-Waves OFP, following the logic of its distributed systems. That is, the system can utilize, without changes, a multitude of new processing stations (workers), as long as they are available. All in all, a system has been implemented that is capable of expanding and introducing new ports to its set of robust and high-resolution forecasts of wave conditions and sea states near and within ports for timely decision-making related to navigation.

It is assumed that Accu-Waves OFP places itself among the state-of-the-art WFSs for Ports Safety Management Systems, assisting more secure navigation towards and inside ports. The goal is to help port managers and ship masters avoid unwanted weather-related ship accidents and vessel bed collisions while mooring, port approaching, ship docking, berth positioning, towing, and harbor dredging procedures take place. Future steps of the Accu-Waves OFP refer to integrating the wave-related danger alerts for large ships with the development of an advisory and forecast service system for safe navigation and mooring in coastal areas per small vessel and fishing boat, too [117–119].

**Supplementary Materials:** The following supporting information can be downloaded at: <https://www.mdpi.com/article/10.3390/jmse12020220/s1>, S1: Characteristic examples of solid boundary classification on the ports' waterfronts for the determination of partial/full wave reflection regimes in Model B's domains; S2: Characteristic details and depiction of the Accu-Waves OFF schematics of WFS model execution in tandem with patrimonial (external) and produced (internal) data flow; S3: Figures of characteristic results by simulations with Model A in 49 globally significant ports are provided. All simulations refer to moderate, rough, and very rough wave conditions and highly detailed depictions of the wave-induced agitation in the areas surrounding the ports (Model A); S4: Figures of characteristic results by simulations with Model B in 22 of the aforesaid 49 ports are provided. All simulations refer to typical (unity for height) wave conditions and highly detailed depictions of the wave-induced agitation inside and around the entrance of the harbor basins (Model B).

**Author Contributions:** Conceptualization, C.M. (Christos Makris), G.S., A.M., M.C., D.Z., V.T., T.K. and C.M. (Constantine Memos); Methodology, C.M. (Christos Makris), V.B., G.S., A.M., Y.A., G.K., T.K. and C.M. (Constantine Memos); Software, C.M. (Christos Makris), A.P., V.B., G.S., Y.K., Y.A., D.M., N.N. and T.K.; Validation, C.M. (Christos Makris), A.P., V.B., G.S., Y.K., Y.A. and G.K.; Formal analysis, C.M. (Christos Makris), V.B., G.S., A.M., Y.A., M.C., G.K., T.K. and C.M. (Constantine Memos); Investigation, C.M. (Christos Makris), A.P., V.B., G.S., Y.K., A.M., Y.A., M.C., G.K. and D.M.; Resources, V.T. and C.M. (Constantine Memos); Data curation, C.M. (Christos Makris), A.P., V.B., G.S., Y.K., D.M. and N.N.; Writing—original draft, C.M. (Christos Makris); Writing—review & editing, C.M. (Christos Makris), A.P., G.S., Y.K., A.M., Y.A., M.C., G.K. and C.M. (Constantine Memos); Visualization, C.M. (Christos Makris), A.P., V.B., G.S. and Y.K.; Supervision, D.Z., V.T., T.K. and C.M. (Constantine Memos); Project administration, C.M. (Christos Makris), M.C., D.Z., V.T., T.K. and C.M. (Constantine Memos); Funding acquisition, D.Z., V.T. and C.M. (Constantine Memos). All authors have read and agreed to the published version of the manuscript.

**Funding:** This research is part of the Accu-Waves project [59], co-financed by the European Union and Greek National Funds through the Operational Program Research-Creat-Innovate (T1EDK-05111).

**Institutional Review Board Statement:** Not applicable.

**Informed Consent Statement:** Not applicable.

**Data Availability Statement:** Data are contained within the article and Supplementary Materials.

**Acknowledgments:** The authors would like to thank the following open-access service providers: (a) the Puertos del Estado SAPO [120] and the SAMOA project [106] for in situ and operational forecast model data at the port of Algeciras; (b) the GFS [98] for weather prediction by NOAA [99]; and (c) the Copernicus Marine Service [34] for both regional and global marine weather forecasts and NRT field data of in situ wave records in the ports of Antwerp and Los Angeles. The Accu-Waves team is also grateful to the Coastal/Hydraulic Engineering consultants "HYDROMARE—S. Christopoulos & Associates Partnership" (Thessaloniki, Greece) and "ECOS Consulting S.A." (Athens, Greece) for collaborating in the WFS performance validation phase.

**Conflicts of Interest:** Authors DZ and GS were employed by the company MarineTraffic [61]. The remaining authors declare that the research was conducted in the absence of any commercial or financial relationships that could be construed as a potential conflict of interest.

## Appendix A

Regarding the evaluation of model operational performance, we have implemented the following statistical measures: correlation, bias/error, and skill performance metrics for the comparison of field/model reference datasets against our own operational forecast simulations. The analysis refers to the time series of any random wave parameter  $A$  (e.g.,  $H_{mo}$ ,  $T_p$ , and  $\varphi_i$ ) or their derivatives, i.e., standard deviations, maxima, averages, etc.).

The classic mean Percent Error,  $PE$  (%), is calculated to compare the bias of statistical measures such as maxima and mean values of simulation results (mod) and in situ observa-

tions (obs). Their desired values are as small as possible, with indicative values of  $PE < 10\%$  for maxima and  $PE < 30\%$  for averages of  $H_{m0}$  and  $T_p$  in our case.

$$PE(\%)_{\max} = 100 \cdot \frac{(A_{\text{mod,max}} - A_{\text{obs,max}})}{A_{\text{obs,max}}} \text{ and } PE(\%)_{\text{mean}} = 100 \cdot \frac{(\overline{A_{\text{mod}}} - \overline{A_{\text{obs}}})}{\overline{A_{\text{obs}}}} \quad (A1)$$

The Pearson product-moment correlation coefficient,  $R_p$ , of two distributions or time-series is the ratio between the covariance of two variables and the product of their standard deviations; thus, it is essentially a normalized measurement of the covariance, such that the result always has a value between  $-1$  and  $1$ . It is actually a measure of estimating the strength of a linear correlation between two random (independent or dependent) variables, distributions, or time series. As with covariance itself, the measure can only reflect a linear correlation of variables and ignores many other types of relationships or correlations. Basically, Pearson’s correlation draws a line of best fit for the bivariate data, and  $R_p$  shows how far all the data points are from that line of best fit (i.e., how well the data fit this new best-fit model). The numeric form of the argument includes a “moment of product,” i.e., the mean value (the first moment from the  $x$ -/ $y$ -axis 0-start point) of the product of the weighted random variables. A value of  $0$  indicates that there is no correlation between the two variables. A value greater than  $0$  indicates a positive correlation. That is, as the value of one variable increases, so does the value of the other variable. A value less than  $0$  indicates a negative correlation. That is, as the value of one variable increases, the value of the other variable decreases. In our case, values in the context of practical operational forecasting applications  $R_p > 0.5$  are considered acceptable,  $R_p > 0.75$  very good, and  $R_p > 0.9$  exceptional.

$$R_p = \frac{\sum_{i=1,N} [(A_{\text{mod},i} - \overline{A_{\text{mod},i}}) \cdot (A_{\text{obs},i} - \overline{A_{\text{obs},i}})]}{\sum_{i=1,N} [(A_{\text{mod},i} - \overline{A_{\text{mod},i}})^2] \cdot \sum_{i=1,N} [(A_{\text{obs},i} - \overline{A_{\text{obs},i}})^2]} \quad (A2)$$

The index  $i = 1, N$  indicates the number of values to compare, and the indices “*mod*” and “*obs*” refer to simulation results and observation data, respectively. The overbar indicates mean values.

The Root-Mean-Square Error (*RMSE*) is the most commonly used measure of the differences between sample or population values predicted by a numerical model (or some estimation/prediction method) and values resulting from field observations. *RMSE* represents the square root of the second moment of a sample of the differences between predicted and observed values of the mean square of these differences. These deviations (differences) are called residuals when calculations are performed only on the sample data used for estimation and are called errors (or prediction errors) when calculated from a comparison of two distributions or timeseries. The *RMSE* serves as a numerical estimator that sums the magnitudes of various prediction errors (in a representation of one data distribution to another) for various records on a single measure with appreciable predictive power. *RMSE* is therefore a measure of accuracy for comparing model prediction errors for a given dataset. The *RMSE* is always non-negative, and a value of  $0$  indicates a perfect fit of the model results to the observed data. In general, a low *RMSE* value is desired. The *RMSE* has the same units as the parameter to be compared (e.g., units  $RMSE_{H_{m0}}$  refer to meters). Practically, it calculates the square root of the mean squared errors between a time series of modeled results and field data. The effect of each individual difference (error) on the *RMSE* index is proportional to the size of the square of the error. Thus, larger differences (deviations or errors) in the time series under consideration have a disproportionately large effect on the *RMSE* value. Consequently, *RMSE* is sensitive to outliers.

$$RMSE = \sqrt{\frac{\sum_{i=1}^N (A_{\text{mod},i} - A_{\text{obs},i})^2}{N}} \quad (A3)$$

$RMSE$  and  $R_p$  are most commonly calculated and presented together, as the 1st only shows how much the time series of model results ( $mod$ ) follows the time series of observations ( $obs$ ), and the 2nd shows how strong the deviation or difference of the characteristic values of the two distributions is.

In coastal hydrodynamics, oceanography, and meteorological forecasting, one of the most complete and reliable indicators of the performance of numerical simulations with respect to observational data is the Willmott Skill Score,  $WSS$ , or Index-of-Agreement,  $IA$  [121]. It is a relative average error or deviation based on the sums of the squares of the differences for each value (sample or population) predicted by a numerical model (or some estimation method) and the values obtained from field observations.

$$WSS = 1 - \frac{\sum_{i=1}^N (|A_{mod,i} - A_{obs,i}|^2)}{\sum_{i=1}^N ( (|A_{mod,i} - \overline{A_{mod,i}}| + |A_{obs,i} - \overline{A_{obs,i}}|)^2 )} \quad (A4)$$

$WSS$  is a statistically bounded measure of the comparison of two time series. By taking the deviations of the two timeseries from each other and also the deviation of each time series from its mean value,  $WSS$  is a good measure of accuracy for comparing model forecast errors of a given dataset. Perfect agreement between the results of a model and the respective observations corresponds to values of  $WSS = 1$ , while for complete disagreement between the two distributions,  $WSS = 0$ .  $WSS$  is dimensionless, always positive, and, in our case, values of  $WSS > 0.5$  are required in evaluation comparisons of the models ( $WSS > 0.5$  is acceptable,  $WSS > 0.75$  is very good, and  $WSS > 0.9$  is exceptional). The effect of each individual difference (error) on the  $WSS$  is also proportional to the size of the squared error. Thus, larger differences (deviations or errors) in the timeseries have a disproportionately large effect on the value of  $WSS$ . Consequently,  $WSS$  is also quite sensitive to outliers. Nevertheless, it is the most complete single-valued numerical representation for forecasting evaluation, yet it requires a long enough time series.

Another evaluation index based on comparison of long-term simulation datasets is the Hit-Rate-of-Percentiles (HRP) index, which is calculated as the sum of the categorical fractions, i.e., the differences between the ranked (from 1st to 100th) percentiles of the simulated and observed random parameter values, compared with an allowed deviation [122]. The latter is usually taken as equal to half of the mean standard deviation of the timeseries of model outputs and field observations, i.e.,  $(\sigma_{Amod} + \sigma_{Aobs})/2$  [97]. The use of HRP-index is intended to check the necessity of possible error correction or bias correction of the simulation results in relation to the existing situation as described by the field observations. HRP-index takes values from 0 to 1, and the simulated results do not need bias correction when  $HRP \geq 0.95$ .

## References

1. World Bank and United Nations Department of Economic and Social Affairs (UNDESA). *The Potential of the Blue Economy: Increasing Long-Term Benefits of the Sustainable Use of Marine Resources for Small Island Developing States and Coastal Least Developed Countries*; World Bank: Washington, DC, USA, 2017.
2. United Nations—Regional Information Centre For Western Europe. *Blue Economy: Oceans as the Next Great Economic Frontier*. Available online: <https://unric.org/en/blue-economy-oceans-as-the-next-great-economic-frontier/> (accessed on 5 December 2023).
3. Hall, A. The Thames Barrier: London's Moveable Flood Defense. In *Environment & Society Portal, Arcadia*; No. 15; Rachel Carson Center for Environment and Society: Munich, Germany, 2014. [CrossRef]
4. Dunton, J.; ZHA Completes Hamburg Flood Project. River Promenade Scheme Tops off Updated Flood-Protection Scheme. 2019. Available online: <https://www.bdonline.co.uk/news/zha-completes-hamburg-flood-project/5101239.article> (accessed on 5 December 2023).
5. Asariotis, R. Climate change impacts on seaports: A growing threat to sustainable trade and development. In *UNCTAD Transport and Trade Facilitation Newsletter N°90—Second Quarter 2021*; Article No. 75; United Nations Conference on Trade and Development (UNCTAD): Geneva, Switzerland, 2021.

6. United Nations Conference on Trade and Development (UNCTAD). *Trade and Development Report 2021. From Recovery to Resilience: The Development Dimension*; United Nations Conference on Trade and Development (UNCTAD): Geneva, Switzerland, 2021.
7. Weintrit, A.; Neumann, T. Marine navigation and safety of sea transportation: STCW, Maritime Education and Training (MET). In *Human Resources and Crew Manning, Maritime Policy, Logistics and Economic Matters*; CRC Press: Boca Raton, FL, USA, 2013.
8. PIANC. *Climate Change Adaptation Planning for Ports and Inland Waterways*; EnviCom WG, PIANC Report n° 178; The World Association for Waterborne Transport Infrastructure, Environmental Commission: Brussels, Belgium, 2020.
9. Becker, A.; Caldwell, M.R. Stakeholder perceptions of seaport resilience strategies: A case study of Gulfport (Mississippi) and Providence (Rhode Island). *Coast. Manag.* **2015**, *43*, 1–34. [[CrossRef](#)]
10. Becker, A.; Ng, A.K.; McEvoy, D.; Mullett, J. Implications of climate change for shipping: Ports and supply chains. *Wiley Interdiscip. Rev. Clim. Chang.* **2018**, *9*, e508. [[CrossRef](#)]
11. Baldauf, M.; Hong, S.B. Improving and assessing the impact of e-Navigation applications. *Int. J. e-Navig. Marit. Econ.* **2016**, *4*, 1–12. [[CrossRef](#)]
12. IMO. *e-Navigation Strategy Implementation Plan*; IMO: London, UK, 2014.
13. Gasparotti, C.; Domnisoru, L.; Rusu, E. Scenarios for the navigation routes in the Black Sea considering the seakeeping safety criteria. In Proceedings of the 14th International Multidisciplinary Scientific GeoConference SGEM, Albena, Bulgaria, 17–26 June 2014.
14. Perera, L.P.; Soares, C.G. Weather routing and safe ship handling in the future of shipping. *Ocean Eng.* **2017**, *130*, 684–695. [[CrossRef](#)]
15. Memos, C.; Makris, C.; Metallinos, A.; Karambas, T.; Zissis, D.; Chondros, M.; Spiliopoulos, G.; Emmanouilidou, M.; Papadimitriou, A.; Baltikas, V.; et al. Accu-Waves: A decision support tool for navigation safety in ports. In Proceedings of the 1st International Scientific DMPCO Conference, Athens, Greece, 8–11 May 2019.
16. Spiliopoulos, G.; Bereta, K.; Zissis, D.; Memos, C.; Makris, C.; Metallinos, A.; Karambas, T.; Chondros, M.; Emmanouilidou, M.; Papadimitriou, A.; et al. October. A Big Data framework for Modelling and Simulating high-resolution hydrodynamic models in sea harbours. In *Global Oceans 2020: Singapore–US Gulf Coast*; IEEE: Piscataway, NJ, USA, 2020; pp. 1–5.
17. Makris, C.; Baltikas, V.; Kontos, Y.; Androulidakis, Y.; Nagkoulis, N.; Kazakis, I.; Karambas, T.; Papadimitriou, A.; Metallinos, A.; Chondros, M.; et al. Integrated modeling of sea-state forecasts for safe navigation near and inside ports: The Accu-Waves platform. In Proceedings of the 31st (2021) International Ocean and Polar Engineering Conference, ISOPE, Rhodes, Greece, 20–25 June 2021; pp. 2307–2314, ISBN 978-1-880653-82-1.
18. Makris, C.; Androulidakis, Y.; Karambas, T.; Papadimitriou, A.; Metallinos, A.; Kontos, Y.; Baltikas, V.; Chondros, M.; Krestenitis, Y.; Tsoukala, V.; et al. Integrated modelling of sea-state forecasts for safe navigation and operational management in ports: Application in the Mediterranean Sea. *Appl. Math. Model.* **2021**, *89*, 1206–1234. [[CrossRef](#)]
19. Myslenkov, S.; Zelenko, A.; Resnyanskii, Y.; Arkhipkin, V.; Silvestrova, K. Quality of the Wind Wave Forecast in the Black Sea Including Storm Wave Analysis. *Sustainability* **2021**, *13*, 13099. [[CrossRef](#)]
20. Rogers, W.E.; Kaihatu, J.M.; Hsu, L.; Jensen, R.E.; Dykes, J.D.; Holland, K.T. Forecasting and hindcasting waves with the SWAN model in the Southern California Bight. *Coast. Eng.* **2007**, *54*, 1–15. [[CrossRef](#)]
21. Allard, R.; Dykes, J.; Hsu, Y.L.; Kaihatu, J.; Conley, D. A real-time nearshore wave and current prediction system. *J. Mar. Syst.* **2008**, *69*, 37–58. [[CrossRef](#)]
22. Dykes, J.D.; Wang, D.W.; Book, J.W. An evaluation of a high-resolution operational wave forecasting system in the Adriatic Sea. *J. Mar. Syst.* **2009**, *78*, S255–S271. [[CrossRef](#)]
23. Singhal, G.; Panchang, V.G.; Lillibridge, J.L. Reliability assessment for operational wave forecasting system in Prince William Sound, Alaska. *J. Waterw. Port Coast. Ocean Eng.* **2010**, *136*, 337–349. [[CrossRef](#)]
24. Bidlot, J.R. Present status of wave forecasting at ECMWF. In *Workshop on Ocean Waves*; ECMWF: Reading, UK, 2012; pp. 25–27.
25. Chawla, A.; Tolman, H.L.; Gerald, V.; Spindler, D.; Spindler, T.; Alves, J.H.G.M.; Cao, D.; Hanson, J.L.; Devaliere, E.M. A multigrad wave forecasting model: A new paradigm in operational wave forecasting. *Weather Forecast.* **2013**, *28*, 1057–1078. [[CrossRef](#)]
26. Rusu, E.; Soares, C.G. Wave modelling at the entrance of ports. *Ocean Eng.* **2011**, *38*, 2089–2109. [[CrossRef](#)]
27. Rusu, L.; Soares, C.G. Evaluation of a high-resolution wave forecasting system for the approaches to ports. *Ocean Eng.* **2013**, *58*, 224–238. [[CrossRef](#)]
28. Rusu, L.; Soares, C.G. Impact of assimilating altimeter data on wave predictions in the western Iberian coast. *Ocean Model.* **2015**, *96*, 126–135. [[CrossRef](#)]
29. Almeida, S.; Rusu, L.; Guedes Soares, C. Data assimilation with the ensemble Kalman filter in a high-resolution wave forecasting model for coastal areas. *J. Oper. Oceanogr.* **2016**, *9*, 103–114. [[CrossRef](#)]
30. Sandhya, K.G.; Nair, T.B.; Bhaskaran, P.K.; Sabique, L.; Arun, N.; Jeykumar, K. Wave forecasting system for operational use and its validation at coastal Puducherry, east coast of India. *Ocean Eng.* **2014**, *80*, 64–72. [[CrossRef](#)]
31. Bonino, G.; Burlando, M.; De Gaetano, P.; Solari, G.; Carmisciano, C.; Iafolla, L. Sea state monitoring and simulation in the “Wind, Ports, and Sea” Project. In Proceedings of the 16th International Congress of the International Maritime Association of the Mediterranean, IMAM, Pula, Croatia, 21–24 September 2015; pp. 875–882.
32. Caires, S.; Marseille, G.J.; Verlaan, M.; Stoffelen, A. North Sea wave analysis using data assimilation and mesoscale model forcing winds. *J. Waterw. Port Coast. Ocean Eng.* **2018**, *144*, 04018005. [[CrossRef](#)]
33. Gautier, C.; Caires, S. Operational wave forecasts in the southern North Sea. In Proceedings of the 36th IAHR World Congress, The Hague, The Netherlands, 28 June–3 July 2015; Volume 1, p. 5.



34. Copernicus Marine Service (CMS). Available online: <http://marine.copernicus.eu> (accessed on 5 December 2023).
35. Tintoré, J.; Pinardi, N.; Álvarez-Fanjul, E.; Aguiar, E.; Álvarez-Berastegui, D.; Bajo, M.; Balbin, R.; Bozzano, R.; Nardelli, B.B.; Cardin, V.; et al. Challenges for sustained observing and forecasting systems in the Mediterranean Sea. *Front. Mar. Sci.* **2019**, *6*, 568. [[CrossRef](#)]
36. WaveForUs (Wave Climate and Coastal Circulation Forecasts For Public Use). Available online: <http://wave4us.web.auth.gr/> (accessed on 5 December 2023).
37. Krestenitis, Y.N.; Androulidakis, Y.; Kombiadou, K.; Makris, C.; Baltikas, V.; Kalantzi, G. Operational oceanographic forecasts in the Thermaikos gulf: The WaveForUs project. In Proceedings of the 12th International Conference on Protection and Restoration of the Environment (PRE), Skiathos, Greece, 29 June–3 July 2014; pp. 313–318.
38. Krestenitis, Y.; Kombiadou, K.; Androulidakis, Y.; Makris, C.; Baltikas, V.; Skoulikaris, C.; Kontos, Y.; Kalantzi, G. Operational Oceanographic Platform in Thermaikos Gulf (Greece): Forecasting And Emergency Alert System For Public Use. In Proceedings of the 36th IAHR World Congress, The Hague, The Netherlands, 28 June–3 July 2015.
39. Baschek, B.; Schroeder, F.; Brix, H.; Riethmüller, R.; Badewien, T.H.; Breitbach, G.; Brügge, B.; Colijn, F.; Doerffer, R.; Eschenbach, C.; et al. The Coastal Observing System for Northern and Arctic Seas (COSYNA). *Ocean Sci.* **2017**, *13*, 379–410. [[CrossRef](#)]
40. Sotillo, M.G.; Cerralbo, P.; Lorente, P.; Grifoll, M.; Espino, M.; Sanchez-Arcilla, A.; Álvarez-Fanjul, E. Coastal ocean forecasting in Spanish ports: The SAMOA operational service. *J. Oper. Oceanogr.* **2020**, *13*, 37–54. [[CrossRef](#)]
41. García-León, M.; Sotillo, M.G.; Mestres, M.; Espino, M.; Fanjul, E.A. Improving Operational Ocean Models for the Spanish Port Authorities: Assessment of the SAMOA Coastal Forecasting Service Upgrades. *J. Mar. Sci. Eng.* **2022**, *10*, 149. [[CrossRef](#)]
42. Fanjul, E.A.; Sotillo, M.G.; Pérez Gómez, B.; Garcia Valdecasas, J.M.; Perez Rubio, S.; Lorente, P.; Rodriguez Dapena, A.; Martinez Marco, I.; Luna, Y.; Padorno, E.; et al. Operational oceanography at the service of the ports. *New Front. Oper. Oceanogr.* **2018**, *27*, 729–736. [[CrossRef](#)]
43. SOCIB Platform. Available online: <https://www.socib.eu/> (accessed on 5 December 2023).
44. Tintoré, J.; Vizoso, G.; Casas, B.; Renault, L.; Garau, B.; Ruiz, S.; Heslop, E.; Torner, M.; Cusí, S.; Martínez-Ledesma, M.; et al. SOCIB: The impact of new marine infrastructures in understanding and forecasting the coastal oceans: Some examples from the Balearic Islands in the Mediterranean Sea. In Proceedings of the CIESM Workshop Monographs n°43, Designing MED-SHIP: A Program for Repeated Oceanographic Surveys—Supetar, Brac Island, Croatia, 11–14 May 2011.
45. Heslop, E.; Tintoré, J.; Rotllan, P.; Álvarez-Berastegui, D.; Fontera, B.; Mourre, B.; Gómez-Pujol, L.; March, D.; Casas, B.; Nolan, G.; et al. SOCIB integrated multi-platform ocean observing and forecasting: From ocean data to sector-focused delivery of products and services. *J. Oper. Oceanogr.* **2019**, *12* (Suppl. S2), S67–S79. [[CrossRef](#)]
46. Campos, R.M.; D’Agostini, A.; França, B.R.L.; Damião, A.L.A.; Soares, C.G. Implementation of a multi-grid operational wave forecast in the South Atlantic Ocean. *Ocean Eng.* **2022**, *243*, 110173. [[CrossRef](#)]
47. Sotillo, M.G.; Mourre, B.; Mestres, M.; Lorente, P.; Aznar, R.; García-León, M.; Liste, M.; Santana, A.; Espino, M.; Álvarez, E. Evaluation of the operational CMEMS and coastal downstream ocean forecasting services during the storm Gloria (January 2020). *Front. Mar. Sci.* **2021**, *8*, 644525. [[CrossRef](#)]
48. Ribeiro, R.B.; Leitão, J.C.; Leitão, P.C.; Puia, H.L.; Sampaio, A.F.P. Integration of high-resolution metocean forecast and observing systems at Port of Santos. In Proceedings of the IX PIANC-COPEDEC, Conference on Coastal and Port Engineering in Developing Countries, Rio de Janeiro, Brazil, 16–21 October 2016.
49. Leitão, J.; Galvão, P.; Leitão, P.; Silva, A. Operational Maritime Weather Forecast for Port Access and Operations Using the Aquasafe Platform. In Proceedings of the IX PIANC-COPEDEC, Conference on Coastal and Port Engineering in Developing Countries, Rio de Janeiro, Brazil, 16–21 October 2016; pp. 16–21.
50. Pinheiro, L.; Gomes, A.; Fortes, C.; Santos, J.A. *Safety System for Ships in Harbours. Technology and Science for the Ships of the Future*; Rizzuto, E., Ruggiero, V., Eds.; IOS Press: Amsterdam, The Netherlands, 2022.
51. Fortes, C.J.E.M. *Transformações não Lineares de Ondas em Portos. Análise pelo Método dos Elementos Finitos. Tese de Doutorament*; IST/DEM: Lisboa, Portugal, 2002.
52. Berkhoff, J. Computation Of Combined Refraction—Diffraction. *Coast. Eng. Proc.* **1972**, *1*, 23. [[CrossRef](#)]
53. Pinheiro, L.V.; Cjem, F.; Santos, J.A.; Fernandes, J.L.M. Numerical software package SWAMS—Simulation of Wave Action on Moored Ships. In Proceedings of the PIANC 3rd Mediterranean Days of Coastal and Port Engineering, Marseille, France, 22–24 May 2013.
54. Mynett, A.E.; Keunig, P.J.; Vis, F.C. The dynamic behaviour of moored vessels inside a harbour configuration. In Proceedings of the International Conference on Numerical and Hydraulic Modelling of Ports and Harbours, Birmingham, UK, 23–25 April 1985.
55. Mavelakis, N.; Kalligeris, N.; Lynett, P.J.; Skanavis, V.L.; Synolakis, C.E. Wave overtopping due to harbour resonance. *Coast. Eng.* **2021**, *169*, 103973. [[CrossRef](#)]
56. IMO. *Report of the Maritime Safety Committee at Its Eighty-Fifth Session*; IMO: London, UK, 2008.
57. Marine Accident Investigation Branch, Department for Transport. *Safety Digest 20; 05-20-2009*; Marine Accident Investigation Branch, Department for Transport: Southampton, UK, 2009.
58. Porretta, M.; Jimenez-Banos, D.; Crisci, M.; Solari, G.; Fiumara, A. *GNSS Evolution for Maritime an Incremental Approach*; European Space Agency: Paris, France, 2016.
59. Accu-Waves Project. Available online: <http://accuwaves.eu/> (accessed on 5 December 2023).

60. Niclasen, B.A.; Simonsen, K.; Magnusson, A.K. Wave forecasts and small-vessel safety: A review of operational warning parameters. *Mar. Struct.* **2010**, *23*, 1–21. [CrossRef]
61. MarineTraffic. Available online: <https://www.marinetraffic.com/> (accessed on 5 December 2023).
62. Rusu, E.; Guedes Soares, C. Modeling waves in open coastal areas and harbors with phase-resolving and phase-averaged models. *J. Coast. Res.* **2013**, *29*, 1309–1325. [CrossRef]
63. Barnes, M.A.; Rautenbach, C. Toward operational wave-current interactions over the Agulhas Current system. *J. Geophys. Res. Ocean* **2020**, *125*, e2020JC016321. [CrossRef]
64. Mortensen, S.B.; Thomsen, F.; Harkin, A.; Shanmugasundaram, S.K.; Simonsen, C.; Nave, R. Web Based Operational System for Optimising Ship Traffic in Depth Constrained Ports. In Proceedings of the 34th PIANC World Congress, Panama City, Panama, 7–11 May 2018.
65. Ducruet, C.; Berli, J.; Spiliopoulos, G.; Zisis, D. Maritime network analysis: Connectivity and spatial distribution. In *Guide to Maritime Informatics*; Springer: Berlin/Heidelberg, Germany, 2021; pp. 299–317.
66. Hellenic Navy Hydrographic Service (HNHS). Available online: <https://www.hnhs.gr/en/> (accessed on 5 December 2023).
67. EMODnet. Available online: <https://rest.emodnet-bathymetry.eu/> (accessed on 5 December 2023).
68. Navionics Platform. Available online: <https://webapp.navionics.com/> (accessed on 5 December 2023).
69. General Bathymetric Chart of the Oceans (GEBCO). Available online: [www.gebco.net](http://www.gebco.net) (accessed on 5 December 2023).
70. Accu-Waves Web-GIS App. Available online: <https://accuwaves.eu/forecast/index.html#> (accessed on 5 December 2023).
71. Makris, C.; Androulidakis, Y.; Baltikas, V.; Kontos, Y.; Karambas, T.; Krestenitis, Y. HiReSS: Storm surge simulation model for the operational forecasting of sea level elevation and currents in marine areas with harbor works. In Proceedings of the 1st DMPCO, Athens, Greece, 8–11 May 2019.
72. Androulidakis, Y.; Makris, C.; Mallios, Z.; Pytharoulis, I.; Baltikas, V.; Krestenitis, Y. Storm Surges during a Medicane in the Ionian Sea. In Proceedings of the Marine and Inland Waters Research Symposium, Porto Heli, Greece, 16–20 September 2022; ISBN 978-960-9798-31-0.
73. Androulidakis, Y.; Makris, C.; Mallios, Z.; Pytharoulis, I.; Baltikas, V.; Krestenitis, Y. Storm surges and coastal inundation during extreme events in the Mediterranean Sea: The IANOS Medicane. *Nat. Hazards* **2023**, *117*, 939–978. [CrossRef]
74. Makris, C.; Androulidakis, Y.; Mallios, Z.; Baltikas, V.; Krestenitis, Y. Towards an Operational Forecast Model for Coastal Inundation due to Storm Surges: Application during Ianos Medicane. In Proceedings of the 9th International Conference on Civil Protection & New Technologies, SafeThessaloniki, Thessaloniki, Greece, 29 September–1 October 2022.
75. Makris, C.; Tolika, K.; Baltikas, V.; Velikou, K.; Krestenitis, Y. The impact of climate change on the storm surges of the Mediterranean Sea: Coastal sea level responses to deep depression atmospheric systems. *Ocean Model.* **2023**, *181*, 102149. [CrossRef]
76. Papadimitriou, A.G.; Chondros, M.K.; Metallinos, A.S.; Memos, C.D.; Tsoukala, V.K. Simulating wave transmission in the lee of a breakwater in spectral models due to overtopping. *Appl. Math. Model.* **2020**, *88*, 743–757. [CrossRef]
77. Papadimitriou, A.; Memos, C.; Atzampou, P.; Chondros, M.; Metallinos, A.; Tsoukala, V. Impact of coastal currents on spectral wave operational models: An application in Accu-Waves. In Proceedings of the 6th IAHR Euro Congress, Virtual, 15–18 February 2021; pp. 441–442.
78. Karambas, T.; Christopoulos, S.; Avgeris, I. HARBOUR\_L: Integrated mathematical model for the design of harbor works. In Proceedings of the 5th Pan-Hellenic Conference on Harbor Works, Athens, Greece, 29 September–1 October 2010.
79. Makris, C.; Karambas, T.; Baltikas, V.; Kontos, Y.; Metallinos, A.; Chondros, M.; Papadimitriou, A.; Tsoukala, V.; Memos, C. WAVE-L: An integrated numerical model for wave propagation forecasting in harbor areas. In Proceedings of the 1st DMPCO Conference, Athens, Greece, 8–11 May 2019.
80. Open TELEMAC Modelling Suite. Available online: <http://www.opentelemac.org/> (accessed on 5 December 2023).
81. Benoit, M.; Marcos, F.; Becq, F. TOMAWAC: A prediction model for offshore and nearshore storm waves. In Proceedings of the IAHR, San Francisco, CA, USA, 10–15 August 1997.
82. Copeland, G.J.M. A Practical Alternative to the Mild-Slope Equation. *Coast Eng.* **1985**, *9*, 125–149. [CrossRef]
83. Watanabe, A.; Maruyama, K. Numerical modeling of nearshore wave field under combined refraction, diffraction and breaking. *Coast Eng. Jpn.* **1986**, *29*, 19–39. [CrossRef]
84. Karambas, T.V.; Bowers, E.C. Representation of Partial Wave Reflection and Transmission for Rubble Mound Coastal Structures. *WIT Trans. Ecol. Environ.* **1996**, *18*, 9.
85. Battjes, J.A.; Janssen, J.P.F.M. Energy loss and set-up due to breaking of random waves. *Coast. Eng.* **1978**, *32*, 569–587.
86. Karambas, T.V.; Samaras, A.G. An integrated numerical model for the design of coastal protection structures. *J. Mar. Sci. Eng.* **2017**, *5*, 50. [CrossRef]
87. Karambas, T.V.; Samaras, A.G. Modelling of Harbour and Coastal Structures. *J. Mar. Sci. Eng.* **2021**, *9*, 1108. [CrossRef]
88. Li, Y.S.; Liu, S.X.; Yu, Y.X.; Lai, G.Z. Numerical modeling of multi-directional irregular waves through breakwaters. *Appl. Math Model.* **2000**, *24*, 551–574. [CrossRef]
89. Yu, Y.X.; Liu, S.X.; Li, Y.S.; Wai, O.W. Refraction and diffraction of random waves through breakwater. *Ocean Eng.* **2000**, *27*, 489–509. [CrossRef]
90. Lee, C.; Suh, K.D. Internal generation of waves for time-dependent mild-slope Equations. *Coast. Eng.* **1998**, *34*, 35–57. [CrossRef]
91. Vincent, C.L.; Briggs, M.J. Refraction—Diffraction of irregular waves over a mound. *J. Waterw. Port Coast. Ocean Eng.* **1989**, *115*, 269–284. [CrossRef]

92. Larsen, J.; Dancy, H. Open Boundaries in Short Wave Simulations—A New Approach. *Coast Eng.* **1983**, *7*, 285–297. [[CrossRef](#)]
93. Karambas, T.V.; Memos, C.D. Boussinesq model for weakly nonlinear fully dispersive water waves. *J. Waterw. Port Coast. Ocean Eng.* **2009**, *135*, 187–199. [[CrossRef](#)]
94. Bruun, P. Stability of breakwater armour layers—Design formulae. *Coast. Eng.* **1989**, *13*, 81–86. [[CrossRef](#)]
95. Thompson, E.F.; Chen, H.S.; Hadley, L.L. Validation of numerical model for wind waves and swell in harbors. *J. Waterw. Port Coast. Ocean Eng.* **1996**, *122*, 245–257. [[CrossRef](#)]
96. Androulidakis, Y.; Kombiadou, K.; Makris, C.; Baltikas, V.; Krestenitis, Y. Storm surges in the Mediterranean Sea: Variability and trends under future climatic conditions. *Dyn. Atmos. Ocean.* **2015**, *71*, 56–82. [[CrossRef](#)]
97. Makris, C.; Galiatsatou, P.; Tolika, K.; Anagnostopoulou, C.; Kombiadou, K.; Prinos, P.; Velikou, K.; Kapelonis, Z.; Tragou, E.; Androulidakis, Y.; et al. Climate change effects on the marine characteristics of the Aegean and Ionian Seas. *Ocean Dyn.* **2016**, *66*, 1603–1635. [[CrossRef](#)]
98. Global Forecast System (GFS). Available online: <https://registry.opendata.aws/noaa-gfs-bdp-pds/> (accessed on 5 December 2023).
99. National Oceanic and Atmospheric Administration (NOAA). Available online: <https://www.ncei.noaa.gov/products/weather-climate-models/global-forecast> (accessed on 5 December 2023).
100. CMS Wave Variables Product. Available online: <https://data.marine.copernicus.eu/products?facets=mainVariables~Wave> (accessed on 5 December 2023).
101. Puertos del Estado. Available online: <https://www.puertos.es/en-us> (accessed on 5 December 2023).
102. Python-Motu Client. Available online: <https://github.com/clstoulouse/motu-client-python> (accessed on 5 December 2023).
103. In Situ Thematic Centre (INSTAC). Available online: <https://marine.copernicus.eu/about/producers/insitu-tac> (accessed on 5 December 2023).
104. Marine Copernicus Product (INSITU\_GLO\_PHYBGCWAV\_DISCRETE\_MYNRT\_013\_030). Available online: [https://data.marine.copernicus.eu/product/INSITU\\_GLO\\_PHYBGCWAV\\_DISCRETE\\_MYNRT\\_013\\_030/description](https://data.marine.copernicus.eu/product/INSITU_GLO_PHYBGCWAV_DISCRETE_MYNRT_013_030/description) (accessed on 5 December 2023).
105. Pre-World Meteorological Organization Global Telecommunication System (Pre-WMO-GTS). Available online: <https://public.wmo.int/> (accessed on 5 December 2023).
106. SAMOA. Available online: <https://www.puertos.es/es-es/proyectos/Paginas/SAMOA.aspx#> (accessed on 5 December 2023).
107. WAMDI Group. The WAM model—A third generation ocean wave prediction model. *J. Phys. Oceanogr.* **1988**, *18*, 1775–1810. [[CrossRef](#)]
108. Aviso+. Available online: <https://www.aviso.altimetry.fr/> (accessed on 5 December 2023).
109. Dask. Available online: <https://dask.org/> (accessed on 5 December 2023).
110. Crontab. Available online: <https://www.computerhope.com/unix/ucrontab.htm> (accessed on 5 December 2023).
111. PostgreSQL. Available online: <https://www.postgresql.org/> (accessed on 5 December 2023).
112. Villefer, A.; Benoit, M.; Violeau, D.; Teles, M.J.; Luneau, C.; Branger, H. Interaction of Short Wind Waves and Swell: An Experimental and Numerical study. In Proceedings of the 39th IAHR World Congress, Granada, Spain, 19–24 June 2022; Volume 19, p. 24.
113. Poseidon Forecast System. Available online: <https://poseidon.hcmr.gr/map> (accessed on 5 December 2023).
114. ABPA Product of Puertos del Estado WFS Infrastructure Algeciras Port. Available online: <https://www.apbawind.oritiayboreas.com/> (accessed on 5 December 2023).
115. Goda, Y. *Random Seas and Design of Maritime Structures*, 3rd ed.; Advanced Series on Ocean Engineering; World Scientific Publishing Company: Singapore, 2010; Volume 33. [[CrossRef](#)]
116. Ricondo, A.; Cagigal, L.; Rueda, A.; Hoeke, R.; Storlazzi, C.D.; Méndez, F.J. HyWaves: Hybrid downscaling of multimodal wave spectra to nearshore areas. *Ocean Mod.* **2023**, *184*, 102210. [[CrossRef](#)]
117. Aditya, N.D.; Sandhya, K.G.; Harikumar, R.; Balakrishnan Nair, T.M. Development of small vessel advisory and forecast services system for safe navigation and operations at sea. *J. Oper. Oceanogr.* **2022**, *15*, 52–67. [[CrossRef](#)]
118. Rusu, L.; Guedes Soares, C. Forecasting fishing vessel responses in coastal areas. *J. Mar. Sci. Technol.* **2014**, *19*, 215–227. [[CrossRef](#)]
119. Sande, J.; Figuero, A.; Tarrío-Saavedra, J.; Peña, E.; Alvarellós, A.; Rabuñal, J.R. Application of an analytic methodology to estimate the movements of moored vessels based on forecast data. *Water* **2019**, *11*, 1841. [[CrossRef](#)]
120. Puertos del Estado SAPO. Available online: <https://www.puertos.es/en-us/oceanografia/Pages/portus.aspx#> (accessed on 5 December 2023).
121. Willmott, C.J.; Robeson, S.M.; Matsuura, K. A refined index of model performance. *Int. J. Climatol.* **2012**, *32*, 2088–2094. [[CrossRef](#)]
122. Schoetter, R.; Hoffmann, P.; Rechid, D.; Schlünzen, K.H. Evaluation and bias correction of regional climate model results using model evaluation measures. *J. Appl. Meteorol. Climatol.* **2012**, *51*, 1670–1684. [[CrossRef](#)]

**Disclaimer/Publisher’s Note:** The statements, opinions and data contained in all publications are solely those of the individual author(s) and contributor(s) and not of MDPI and/or the editor(s). MDPI and/or the editor(s) disclaim responsibility for any injury to people or property resulting from any ideas, methods, instructions or products referred to in the content.